Article

Galectin-3 Regulates γ-Herpesvirus Specific CD8 T Cell Immunity

Manpreet Kaur,
Dhaneshwar
Kumar, Vincent
Butty, ..., Gerald R.
Fink, Hidde L.
Ploegh, Sharvan
Sehrawat

hidde.ploegh@childrens.
harvard.edu (H.L.P.)
sharvan@iisermohali.ac.in
(S.S.)

HIGHLIGHTS

A comprehensive
transcriptomic analysis on
γ-HV-expanded TN cells
was performed

CD8 T cells upregulated
Gal-3 that migrated
intracellularly toward
immune synapse

Stimulated naive and
memory cells displayed
galectin-3 recruitment to
immune synapse

γ−HV-infected Gal-3 KO
mice mounted better
CD8+ T cells and
controlled virus better

Article

Galectin-3 Regulates γ-Herpesvirus Specific CD8 T Cell Immunity

Manpreet Kaur,[1] Dhaneshwar Kumar,[1] Vincent Butty,[2] Sudhakar Singh,[1] Alexandre Esteban,[2] Gerald R. Fink,[2] Hidde L. Ploegh,[2,3,*] and Sharvan Sehrawat[1,4,*]

SUMMARY

To gain insights into the molecular mechanisms and pathways involved in the activation of γ-herpesvirus (MHV68)-specific T cell receptor transnuclear (TN) CD8^{+} T cells, we performed a comprehensive transcriptomic analysis. Upon viral infection, we observed differential expression of several thousand transcripts encompassing various networks and pathways in activated TN cells compared with their naive counterparts. Activated cells highly upregulated galectin-3. We therefore explored the role of galectin-3 in influencing anti-MHV68 immunity. Galectin-3 was recruited at the immunological synapse during activation of CD8^{+} T cells and helped constrain their activation. The localization of galectin-3 to immune synapse was evident during the activation of both naive and memory CD8^{+} T cells. Galectin-3 knockout mice mounted a stronger MHV68-specific CD8^{+} T cell response to the majority of viral epitopes and led to better viral control. Targeting intracellular galectin-3 in CD8^{+} T cells may therefore serve to enhance response to efficiently control infections.

INTRODUCTION

Timely induction of an adaptive immune response and the formation of effective immunological memory are essential for protective immunity against infectious diseases (Ahmed and Gray, 1996). Appropriately activated CD8^{+} T cells help control intracellular pathogens through recognition of peptides derived from pathogens in the context of class I major histocompatibility complex (MHC) products. Induction of a CD8^{+} T cell response requires the processing of three types of signal, delivered via peptide-MHC (p-MHC) complexes, co-stimulatory molecules, and the prevailing cytokine milieu. Activated CD8^{+} T cells expand to become effector cells that lyse their targets and so eliminate the intracellular pathogen (Zinkernagel, 1996). Several mechanisms then engage to regulate this response to limit possible damage caused by hyperactive immune cells (Ahmed and Gray, 1996).

Most pathogens establish an intricate relationship, manifested at many stages, with their host to ensure transmission, including invasion and the establishment of a productive infection. Barring a few exceptions, pathogen-specific CD8^{+} T cell responses are usually polyclonal in nature and recognize multiple epitopes specified by the invading pathogen (Wong and Pamer, 2003). This applies in particular to complex pathogens such as poxviruses and herpesviruses (HVs) in their natural hosts (Amanna et al., 2006; Freeman et al., 2010; Gredmark-Russ et al., 2008; Moutaftsi et al., 2006). γ-HVs are species-specific pathogens, and therefore analysis of anti-γ-HV responses requires a natural host. Infection of mice with murine herpesvirus 68 (MHV68) is one of the most accessible model systems to study anti-γ-HV immunity and immunopathology (Nash and Dutia, 2008; Nash et al., 2001; Sehrawat et al., 2018). Various immune mediators induced in MHV68-infected mice display similarity to those induced during γ-HV infections in humans (Barton et al., 2011). Previously, we generated MHV68-specific CD8^{+} T cell receptor transnuclear (TCR TN) mice by somatic cell nuclear transfer approach to investigate the contribution of CD8^{+} T cells to viral control (Sehrawat et al., 2012). TCR TN mice use the physiological rearrangements of the endogenous antigen receptor loci. Therefore, CD8^{+} TCR TN mice are likely to yield physiologically relevant primary T cell populations to investigate their responsiveness during infection (Kirak et al., 2010; Sehrawat et al., 2012).

The efficiency with which T cells engage antigen-presenting cells (APCs) in an immunological synapse regulates their activation, differentiation, and functionality (Dustin and Cooper, 2000; Fooksman et al., 2010; Mempel et al., 2004; Viola et al., 1996). The components of the immune synapse, such as the TCR, co-receptors (CD3 with all its subunits), lineage differentiation surface glycoproteins such as CD4 and CD8, adhesion molecules, and phosphatases (CD45), are extensively decorated with carbohydrates (Qian and Weiss, 1997). Therefore carbohydrate-binding proteins (lectins) such as members of the galectin family

may be critical in the formation, stabilization, and disassembly of the immunological synapse. Galectins may also affect the differentiation of T cells (Hsu et al., 2009). Galectins bind to a variety of glycosylated proteins, expressed intracellularly or on the cell surface (van Kooyk and Rabinovich, 2008). Such interactions are either mediated by galectin-glycan lattices or through specific receptor-ligand pairs (van Kooyk and Rabinovich, 2008). At least 15 different galectins have been identified, and all have at least one conserved carbohydrate recognition domain (CRD), consisting of approximately 130 amino acids (Rabinovich et al., 2002). Although galectins do not have classical secretory signals, some can nonetheless be released into the extracellular space (Hughes, 1999).

We performed RNA sequencing (RNA-seq) on MHV68-specific naive and activated CD8$^+$ TCR TN T cells to gain insight into their function and phenotype. Activated TN cells isolated from virus-infected mice differentially expressed several thousand transcripts. We discovered several novel transcripts whose function remains to be fully defined in T cell biology. Among these, we found strong upregulation of galectin-3 in the virus-specific CD8$^+$ T cells activated and expanded in response to the MHV68 infection. We, therefore, investigated the role of galectin-3 in the activation of CD8$^+$ T cells during MHV68 infection, as its contribution in anti-viral CD8$^+$ T cell immunity remains ill defined. Some studies have suggested a regulatory role of galectin-3 in CD8$^+$ T cell responses in autoimmune diseases and tumors (Gordon-Alonso et al., 2017; Kuo et al., 2015). In the tumor microenvironment, the extracellular galectin-3 interacted with effector molecule, interferon (IFN)-γ, owing to its extensive glycosylation and dampened its protective function against the developing tumor (Gordon-Alonso et al., 2017). We demonstrate that galectin-3 is recruited at the immunological synapse but predominantly acts intracellularly within CD8$^+$ T cells engaged to cognate peptide displayed by MHC I both during the primary and memory response. CD8$^+$ T cells lacking galectin-3 expanded more vigorously and produced enhanced cytokines when compared with wild-type (WT) CD8$^+$ T cells. Furthermore, galectin-3 knockout (KO) mice mounted a stronger virus-specific CD8$^+$ T cell response against most of the investigated epitopes and controlled virus better. Therefore, modulating the galectin-3 response pattern in CD8$^+$ T cells may serve as a strategy to enhance their function.

RESULTS

Phenotype of Naive and MHV68-Stimulated TCR TN CD8$^+$ T Cells

We compared the transcriptome of activated MHV68-specific ORF8 TCR TN CD8$^+$ T cells (Sehrawat et al., 2012) with their naive counterparts to gain insight into their function and phenotype. Both naive and activated CD8$^+$ T cells were obtained from genetically comparable TCR TN mice (see schematic, Figure 1A). TN CD8$^+$ T cells expanded massively in response to MHV68 infection in congenic (CD45.1) mice that received 50 $\times$ 10^3 open reading frame (ORF) TN cells before infection. At 6 days post infection (dpi), 35%–40% of the total CD8$^+$ T cells in spleens of infected mice were composed of donor ORF8 TCR TN cells. Cells that responded to viral infection had increased surface display of the activation markers such as CD44 and program death 1 (PD1) (Figure 1B), demonstrating a fresh recruitment of these cells in the course of the infection. Most of these cells produced IFN-γ in Intracellular cytokine staining (ICCS) assays (Sehrawat et al., 2012). We performed fluorescence-activated cell sorting (FACS) of activated ORF8 TCR TN CD8$^+$ T cells for further analysis as shown in Figure 1B.

RNA-Seq Data and Assessment of Its Quality

FACS-purified naive cells and activated cells were processed for RNA isolation. Libraries were constructed and subjected to paired-end sequencing. Approximately 1 million reads of excellent quality for each sample were obtained (Figures 1C and S1A). A high fraction of uniquely mapping reads having a minimal amount of ribosomal RNA sequences were obtained. Further analysis of RNA-seq data showed a high percentage of junction reads, good exon/intron as well as exon/intergenic ratios, and minimal 3'/5' bias in sequence coverage (Figure S1A). The expression of some genes, as exemplified by β_2m, class I MHC, and Tap1, did not change between naive and activated TN cells and served as a point of reference with which to compare the observed changes (Figure S1B). Normalized RPKM and a log$_2$ fold change of different genes from naive and activated TN cells are shown in Table S1 and in a scatterplot (Figure 1C). Ensembl entries (n = 11,689) also present in our RNA-seq data with more than 5 reads in either samples are shown in a scatterplot (Figure 1C). The extent of differential expression of a large majority of genes in activated when compared with naive ORF8 TCR TN CD8$^+$ T cells was up to less than 2-fold (Figure 1D). Top hits that were differentially expressed in TN cells are discussed in the following sections.
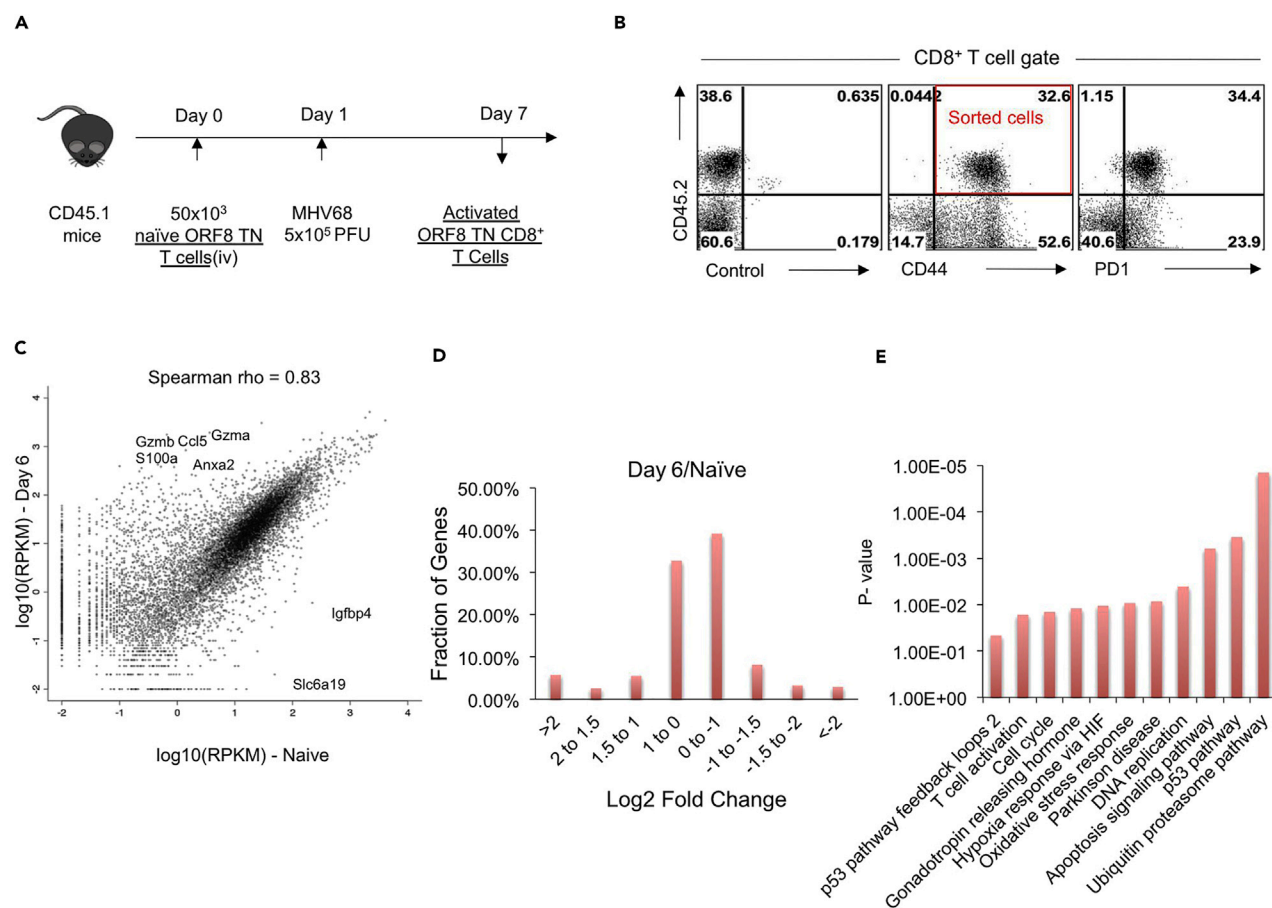
Figure 1. RNA-Seq Analysis of Naive and MHV68-Expanded ORF8 TCR TN CD8$^+$ T Cells

(A) Schematic of the experiment. 50 × 10^3 Rag1$^{-/-}$ K^b-ORF8 TCR TN CD8$^+$ T cells were adoptively transferred in CD45.1 congenic C57BL/6 mice, and recipients were infected with 5 × 10^5 plaque-forming unit (PFU) of MHV68 i.p. On 6 dpi, spleens were isolated and single-cell suspensions were analyzed flow cytometrically using a panel of indicated cell surface markers.

(B) Representative FACS plots showing the phenotypic markers expressed by CD45.2-positive cell (Rag1$^{-/-}$ K^b-ORF8 TCR TN CD8$^+$ T cells) activated and expanded in response to viral infection.

(C) Sorted CD45.2$^+$ CD44^{hi} cells that were expanded due to MHV68 infection and their naive counterparts were used for RNA sequencing. Scatterplot shows the differential expression of transcripts in naive and 6 dpi activated TN CD8$^+$ T cells.

(D and E) (D) Bar diagram shows the extent by which the fraction of genes are differentially expressed. (E) Gene ontology panther pathway analysis of differentially expressed transcripts in ORF8 TCR TN CD8$^+$ T cells for the biological processes represented.

Analysis of Transcriptome of Naive and Activated TCR TN CD8$^+$ T Cells

Our initial analyses involved the number of reads for the α (TRAV10N801, TRAJ33*01) and β chains (TRBV31*01, D1*01 and TRBJ2-2*01) of the specific TCR used by ORF8 TCR TN CD8$^+$ T cells (Sehrawat et al., 2012). We found a high degree of sequence coverage across the expected TCR α and β chains (Figure S1C). As TCR expression is downregulated in stimulated T cells in the acute phase of response, fewer reads were obtained for the TCR chains in activated CD8$^+$ T cells (Figure S1C).

Of the several thousand transcripts differentially expressed in activated TN CD8$^+$ T cells, many have not been reported to exhibit a similar expression pattern Table S1. We also compared our RNA-seq data with the transcriptome of two of the commonly used CD8$^+$ TCR transgenic (tg) mice (OT1 and P14) as these mice have provided excellent insights into the differentiation pathways of antigen-specific CD8$^+$ T cells (Best et al., 2013; Wherry et al., 2007). The comparison revealed that more transcripts were differentially expressed in TCR TN CD8$^+$ T cells (Figures S1D and S1E, Table S1). The varying TCR affinities of TN T cells when compared with the tg cells, the usage of endogenous TCR loci for receptor assembly by TN cells when compared with other tg cells, and the influence of microenvironment generated during

respective infection may all contribute to the observed differences. Varying affinity of peptide recognition by TCRs of TN and tg cells was shown by tetramer dissociation assays in an earlier work (Sehrawat et al., 2012). The possible contribution of differences in microenvironment and co-stimulatory molecules, as are expected to occur in a natural γ-HV infection, versus antigen delivery by other means, was not investigated further.

Multiple transcripts were clustered in different pathways such as cell cycle progression, apoptosis signaling, DNA replication, hypoxia response via hypoxia-inducing factors, oxidative stress response, T cell activation, the ubiquitin-proteasome pathway, and the p53 pathway (Figure 1E). A compilation of different biological processes represented by differentially expressed transcripts in ORF8 TN cells is shown in Tables S2 and S3. Genes encoding different classes of proteins that were differentially expressed by activated TN cells included nucleic acid-binding proteins, G-protein-coupled receptors, ribosomal proteins, transcription factors, ligand-gated ion channels, signaling molecules and adaptors, chaperones, growth factors, cell adhesion molecules, cytoskeletal proteins, splicing factors, extracellular matrix, as well as structural proteins (Figures S2A and S2B). Our RNA-seq data showed that transcripts for many genes were differentially expressed in activated TN cells associated with the effector functions of $CD8^+$ T cells (Figures 1C and Table S1). We validated the altered expression of some of the genes differentially expressed in activated TN cells by cytofluorometry, and these include CD62L, TIM-3, PD1, CD44, CCR7, galectin-3, and IFN-γ at the protein product level (Figures 1B and S4A–S4D; Sehrawat et al., 2012).

Expression Profile of MHV68-Specific $CD8^+$ T Cells upon Virus Infection

$CD8^+$ T cells exponentially expand during the acute phase of infection and acquire a differentiation program that helps them migrate to the site(s) of infection to control infection (Kaech and Cui, 2012). Several genes differentially expressed by activated ORF8 TN cells represent such events (see Table S1 for a complete listing). In brief, transcripts for genes that encode for proinflammatory cytokines such as IFN-γ (up by 40-fold); granzymes B, A, and K (up by 300- to 900-fold); chemokine receptors such as CCR5 (up by 77 fold); and the chemokine RANTES (up by 300-fold) were highly upregulated in activated TN T cells when compared with their naive counterparts. Annexin II, a vesicular protein that facilitates extracellular transport of other proteins, was highly expressed (up by 250-fold) in activated TN cells, suggesting its critical role in effector functions of $CD8^+$ T cells. Similarly, transcription factors that promote cellular proliferation and help produce several effector molecules were highly upregulated in expanded TN T cells. Some examples include Tbet (up by 93-fold), Zbtb32 (up by 67-fold), polycomb-group repressive complex 1 (up by 40-fold), and E2f2 (up by 35-fold). Other genes that are associated with activation and fate determination of $CD8^+$ T cells such as *klrc1* (up by 54-fold), *lag3* (up by 48-fold), *klrg1* (up by 30-fold), *havrc2* (TIM-3: up by 30-fold), *pdcd1* (PD1: up by 26-fold), and *ctla4* (CTLA4: up by 17-fold) were also significantly upregulated in TN cells. Genes responsible for encoding Ca^{++}-binding proteins such as those of the S100 family (*s100a6, s100a4, s100a9, s100a10, s100a8*) were upregulated up to 100-fold by activated TN T cells. Most of these proteins are involved in differentiation and cell cycle progression and are known to modulate tubulin polymerization (Donato et al., 2013). Genes encoding galectin-1 (*lgals1*: up by 87-fold) and galectin 3 (*lgals3*: up by 140-fold) were among the highly upregulated genes in activated TN T cells. In this study, we decided to investigate the role of galectin-3 in anti-γ-HV $CD8^+$ T cell immunity, as will be described below.

Numerous genes were downregulated in virus-reactive activated ORF8 TN T cells compared with naive TN cells (Table S1). The extent of downregulation was more than 40-fold for five genes, between 20- and 40-fold for six genes, between 10- and 20-fold for approximately 40 genes, between 5- and 10-fold for more than 100 genes, and up to 2-fold for several thousand genes (Figures 1C and 1D and Table S1). One of the most downregulated genes in activated TN cells was *igfbp4* (down by 131-fold), which encodes insulin-like growth factor-binding protein 4. This molecule is involved in the differentiation of helper cells such as Th1, Th17, and regulatory T cells (Miyagawa et al., 2017). Whether or not this molecule plays a role in the differentiation of $CD8^+$ T cells has not been investigated. Genes that encode for transporters of amino acids (*slc6a19*: down 42-fold, *slc6a5*: down 37-fold, *slc2a7*: down 11-fold) were highly downregulated in activated TN T cells compared with ion transporters (*slc4a1, slc7a1*), urea transporters (*slc14a1*), and carbohydrate transporters (*slc35b3*). This suggests that during the acute phase of a $CD8^+$ T cell response, fate and function are greatly influenced by transport and metabolism of amino acids or by redox potential (Böhmer et al., 2005; Lin et al., 2015). The gene for the actin regulator FAM101B was also downregulated in activated TN cells. FAM101B localizes to the perinuclear space and helps stabilize perinuclear actin filament bundles (Gay et al., 2011). Its function in $CD8^+$ T cell differentiation remains to be investigated. A gene

st6gal1, which encodes ST6 β-galactoside α-2,6-sialyltransferase, was downregulated by 22-fold in activated TN cells, which might suggest a differential modification, particularly the capping of molecules such as CD45 with α-2,6-sialic acid during development of T cells in the thymus, when compared with their glycosylation profile during their HV-induced activation in the periphery (Elliott et al., 2018). Many such issues remain less well studied. The glycosylation status of different proteins in CD4+ T cells is known to control their differentiation program, but studies investigating its role in CD8+ T cell differentiation are limited (Toscano et al., 2007). Interleukin (IL)-7R (*il7r*: down by 25 fold) specifically marks precursors of memory CD8+ T cells during the acute phase of infection (Kaech et al., 2003). Similar to its expression pattern, genes for other molecules such as GPR114 (*gpr114*: down by 17-fold), IFN-γR2 (*ifngr2*: down by 16-fold), vasoactive intestinal peptide receptor 1 (*Vipr1*: down by 15-fold), interferon-inducible members of the *schlafen* family (*slfn5*: down by 15-fold), adhesion molecule with Ig-like domain 2 (*amigo2*: down by 14-fold), and TNF receptor superfamily member 25 (*tnfrsf25*: down by 14-fold) were among those downregulated in activated TN CD8+ T cells. Many of these molecules have been implicated in T cell differentiation, but the role of others remains to be explored (Geserick et al., 2004; Slebioda et al., 2011).

Apart from the genes described in this section, several thousand differentially expressed genes are listed in Tables S1 and S4.

Network Analysis for Significantly Differentially Expressed Genes during Activation of MHV68-Specific TCR-TN CD8+ T Cells

It is technically challenging to explore in depth all the genes whose expression changes significantly upon TN cell activation. Therefore, we performed a network analysis for those genes that were highly differentially expressed in naive and activated TN cells (Figure S3). In brief, the STRING network analysis revealed 229 nodes, which interacted with each other by 7,892 edges, and the average node degrees was 68.9. The average local clustering coefficient was found to be 0.721. A value of clustering coefficient nearing 0 suggests no clustering, whereas a value of 1 represents maximal clustering (Elliott et al., 2018). Many of the genes present in the network have been studied during differentiation of T cells expanded during infectious agents (Best et al., 2013; Wherry and Ahmed, 2004; Wherry et al., 2007). We focused our further analysis on the family of galectins that have critical role in immune responses during infection, autoimmunities, and cancers. We generated a STRING network for Lgals encoded by lgals genes (Figures S3B and S3D). Two such networks were obtained in which Lgals3 and Lgals1 served as hub genes. The network with Lgals3 revealed 10 interacting partners, whereas the one with Lgals1 revealed only six interacting partners each having a high protein protein interaction (PPI) enrichment score and p value less than 1.0×10^{-16} (Figures S3B and S3C). Lgals3 had more interacting partners and additionally included many partners of Lgals1. Given its critical role during activation of T cells, we chose galectin-3 for elucidating its role in CD8 T cell response induction during γ-HV infection (Figure S3D) (Hsu et al., 2009).

Expression of Galectin-3 in Activated CD8+ T Cells

We analyzed and compared the transcriptional expression profile of all the members of galectin family in naive and the virus-activated ORF8 TCR TN CD8+ T cells (Figure 2A). Galectin-3 showed increased expression in activated TN T cells (up ~140-fold) (Figures 2A and 2B). The expression of galectin-3 by polyclonal CD8+ T cells induced during γ-HV infection in the spleen is shown in Figure 2C. We also measured expression of galectin-3 protein in adoptively transferred TN cells and in endogenous CD8+ T cells that expanded in response to MHV68 infection in recipient congenic (CD45.1) mice (Figure 2D). A few naive CD8+ T cells (less than 10%) showed galectin-3 expression, whereas all virus-specific endogenous (~2% of total CD8+ T cells) as well as donor TN CD8+ T cells (97.4% of total CD8+ T cells) scored positive for galectin-3 expression 6 dpi in spleen samples (Figure 2D). Endogenous MHV68-ORF8-specific CD8+ T cells were likewise analyzed for galectin-3 expression in the absence of an adoptive transfer. A large majority of H-2Kb-ORF8-Tet+ CD8+ T cells in peripheral blood (Figure 2E) and spleen (data not shown) expressed galectin-3.

To investigate the kinetics of galectin-3 protein induction in CD8+ T cells, we stimulated sorted CD8+ T cells from WT mice with anti-CD3 and anti-CD28 antibodies. Intracellular and extracellular expression of galectin-3 was measured (Figures 2F and S4D). Upon activation, CD8+ T cells upregulated the intracellular pool of galectin-3 to a larger extent when compared with its surface expression (Figure S4D). More CD8+ T cells expressed intracellular galectin-3 (~30% at 16 hr and more than 70% at 70 hr post stimulation) (Figure 2F). As expected, a large majority of CD8+ T cells were additionally upregulated CD69 upon stimulation (Figure 2F). The total galectin-3-expressing cells as detected in these assays are likely to include the cells
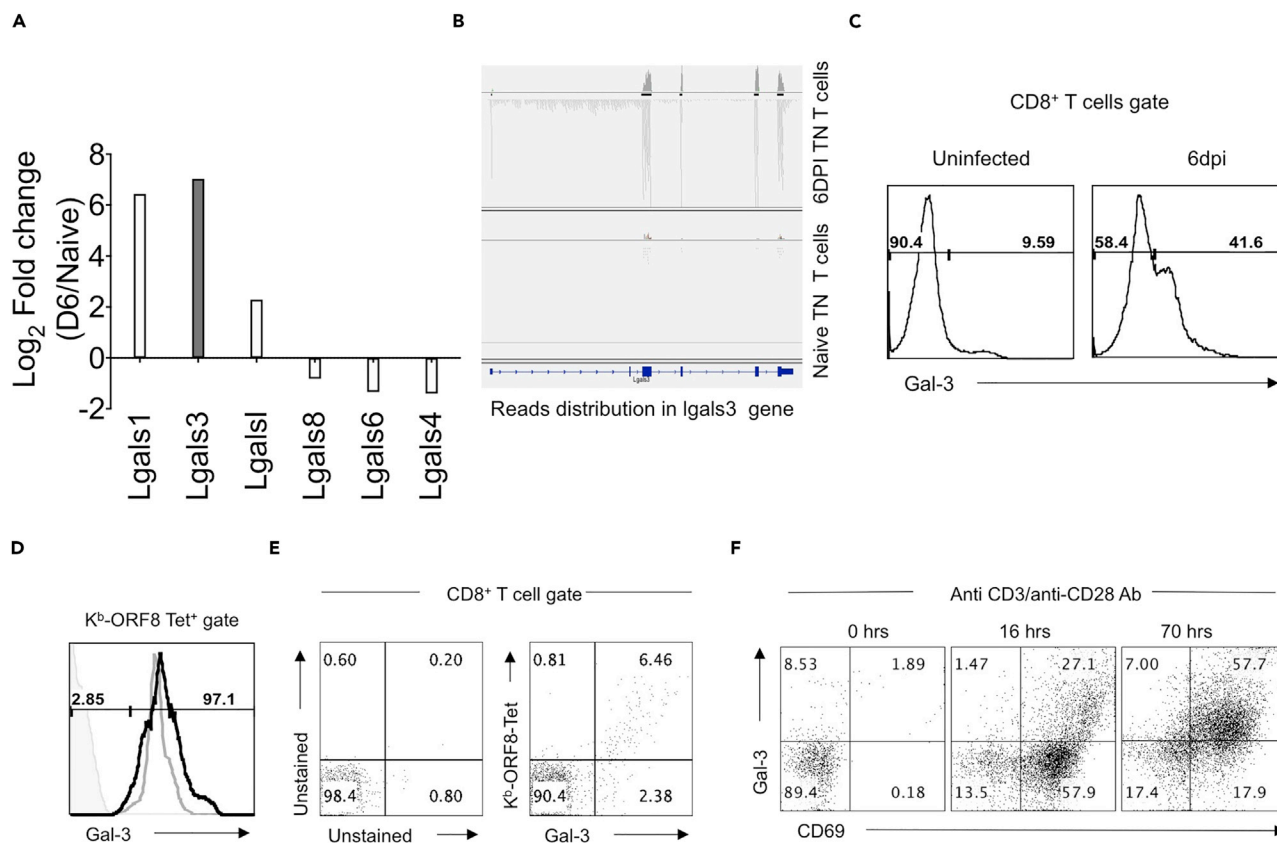
Figure 2. CD8^{+} T Cells Upregulate Galectin-3 Expression upon TCR and Co-receptor Ligation

(A) Bar diagram shows a fold change in the expression of transcripts for different galectins in naive and activated TCR TN CD8^{+} T cells as a result of MHV68 infection as analyzed from RNA-seq data.

(B) Integrative genomics viewers (IgV) snapshots to show the frequency of reads encompassing the exons (filled rectangles on the bottom line) versus intron (line without rectangles) of galectin-3 gene (Lgals3) in activated ORF8 TN CD8^{+} T cells (6 dpi) and their naive counterparts.

(C) 50 × 10^{3} TN cells were transferred in congenic CD45.1 mice, and 6 days later the expression of galectin-3 was measured on total CD8^{+} T cells.

(D) Galectin-3 expression was measured flow cytometrically in H-2K[b]-KNYIEFEKL-specific CD8^{+} T cells on 6 dpi to measure intracellular galectin-3 expression. The staining with specific antibodies followed Fc receptors blocking. Bold black line in overlaid histogram represents expression of galectin-3 in CD45.1^{+} cells (endogenous CD8^{+} T cells; ~2% of total CD8^{+} T cells), and gray line represents galectin-3 expression in donor CD45.2^{+}cells (TCR TN cells; 97.3% of total CD8^{+} T cells).

(E) C57BL/6 mice were infected with MHV68, and CD8^{+} T cells from peripheral blood were analyzed for intracellular galectin-3 at 10 dpi. FACS plots show the expression of galectin-3 in K[b]-ORF8-tetramer-positive cells. The protocol used does detect cell surface and intracellular pool of galectin-3.

(F) Purified CD8^{+} T cells were stimulated by soluble anti-CD3 (1 μg/mL) and anti-CD28 (1 μg/mL) in the presence of IL-2 in a round-bottomed plate for 16 and 70 hr. The expression of surface CD69 and intracellular galectin-3 was analyzed. Representative FACS plots are shown for all the experiments.

expressing surface galectin-3 as well. Therefore, we measured its expression in both the permeabilized and intact cells (Figure S4D). These experiments revealed a predominant intracellular expression of galectin-3 in activated cells (Figure S4D).

Galectin-3 Is Recruited at the Immunological Synapse during CD8^{+} T Cell Activation

During induction of CD8^{+} T cell responses, the TCR recognizes the p-MHC complex that is central to the immunological synapse. Other constituents are recruited subsequently. Most proteins that participate in the immune synapse are glycosylated. Galectin-3, through its CRD, could interact with them to influence T cell activation (Chen et al., 2009). We performed confocal microscopy to investigate whether galectin-3 expressed either at the basal level in CD8^{+} T cells or upregulated after stimulation of naive and memory CD8^{+} T cells is recruited to the immunological synapse. The extent of co-localization was measured and quantified as described (Dunn et al., 2011). After the TCR is ligated with cognate ligand, signaling events create docking sites for the cytosolic adapter molecule Zap70, which is recruited upon phosphorylation of ζ-chain of the co-receptor. We stimulated antigen-specific OT1 cells with immobilized
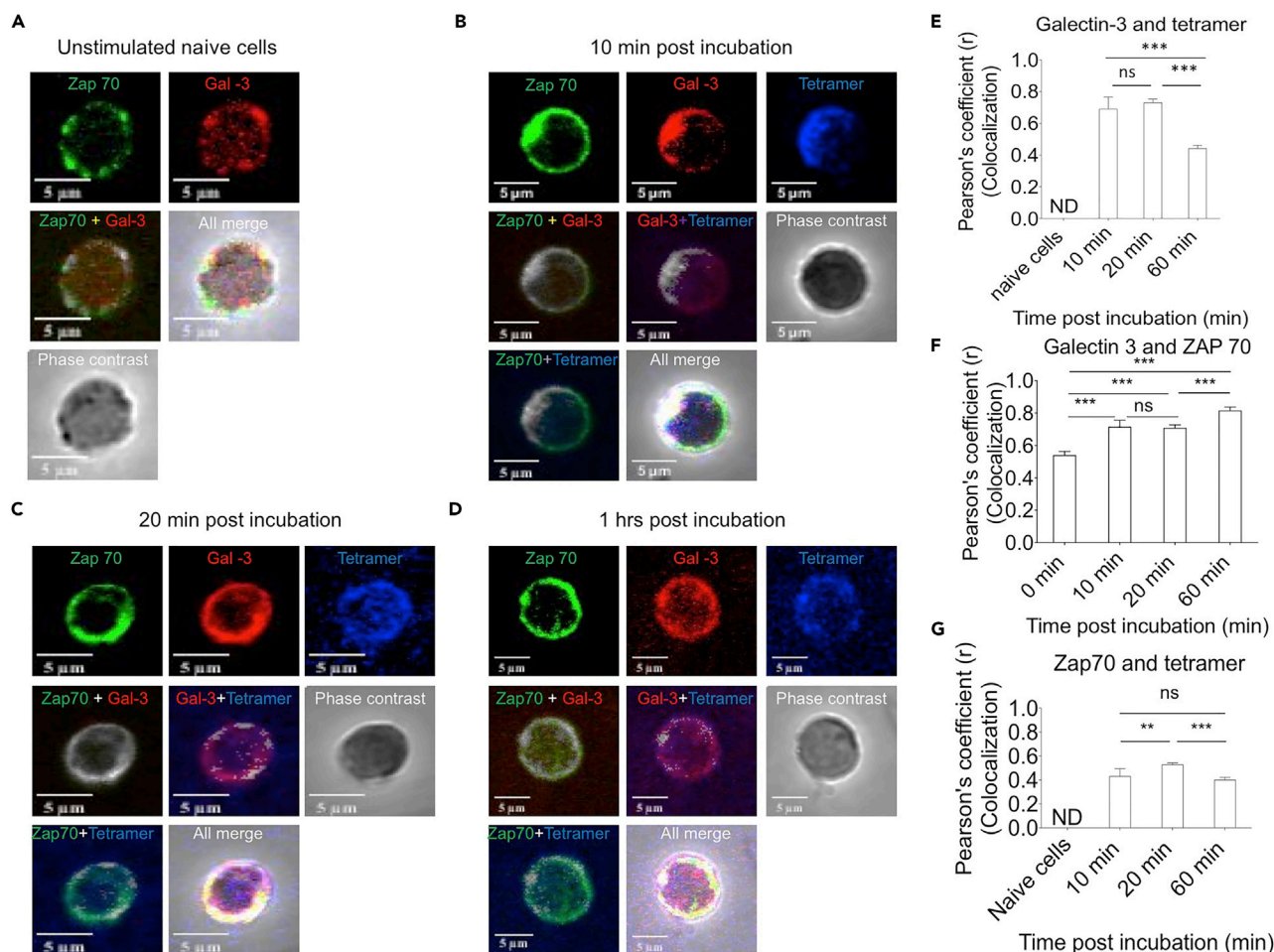
Figure 3. Galectin-3 Expressed by TCR-Stimulated CD8^{+} T Cells Is Recruited at Immunological Synapse

Antigen-specific CD8^{+} T cells from OT1 mice were negatively selected by Magnetically activated cell sorting (MACS) purification and subsequently stimulated with specific peptide-loaded class I MHC tetramer (H-2K[b]-SIINFEKL-Tetramer-APC conjugated and immobilized on coverslips).

Purified CD8^{+} T cells were added onto coverslips and incubated for varying times. At indicated time, cells were stained for different molecules, and confocal images were acquired as described in Transparent Methods.

(A) OT1 cells incubated for 60 min on coverslips in the absence of H-2K[b] tetramers were analyzed for different markers. Representative micrographs for individual staining and co-localization of Zap70, galectin-3, and tetramer are shown.

(B–D) OT1 cells incubated for 10 min (B), 20 min (C), and 60 min (D) on coverslips in the presence of H-2K[b] tetramers were similarly analyzed for different markers. Representative images for each group are shown.

(E–G) Cumulative data for co-localization experiments obtained from more than 30 different cells is shown. Tukey multiple comparison test was used to determine the level of significance. Colocalization of galectin-3 and tetramer (E), galectin-3 and zap70 (F) and zap70 and tetramer (G) at different time points post incubation. ns, non-significant, **p <0.01 and ***p<0.001.

H-2K[b]-SIINFEKL-tetramer-allophycocyanin and stained for galectin-3 and Zap70. Unstimulated cells served as controls. A diffuse and low level of expression for Zap70 was seen in naive cells (Figures 3A, 3E, and 3F). The extent of co-localization of galectin-3 with Zap70 was ~50% in unstimulated cells. Within 10 min of incubation with MHC I tetramer, co-localization of galectin-3 with the MHC I tetramer increased (~70 percent), as did galectin-3 with Zap70 (more than 70%) (Figure 3B). The extent of co-localization remained high at 20 min but began to diffuse at 60 min post stimulation (Figures 3C and 3D). Diffuse staining for Zap70 was apparent at 60 min (Figure 3D). Upon TCR stimulation, galectin-3 expressed at basal level in CD8^{+} T cells is co-localized with Zap70.

Next, we investigated whether galectin-3 upregulated in previously stimulated CD8^{+} T cells is recruited to the immunological synapse upon their re-stimulation. To this end, OT1 cells were stimulated *in vitro* using anti-CD3 and anti-CD8^{+} antibodies for 72 hr. These cells were then co-cultured with SIINFEKL-pulsed Bone
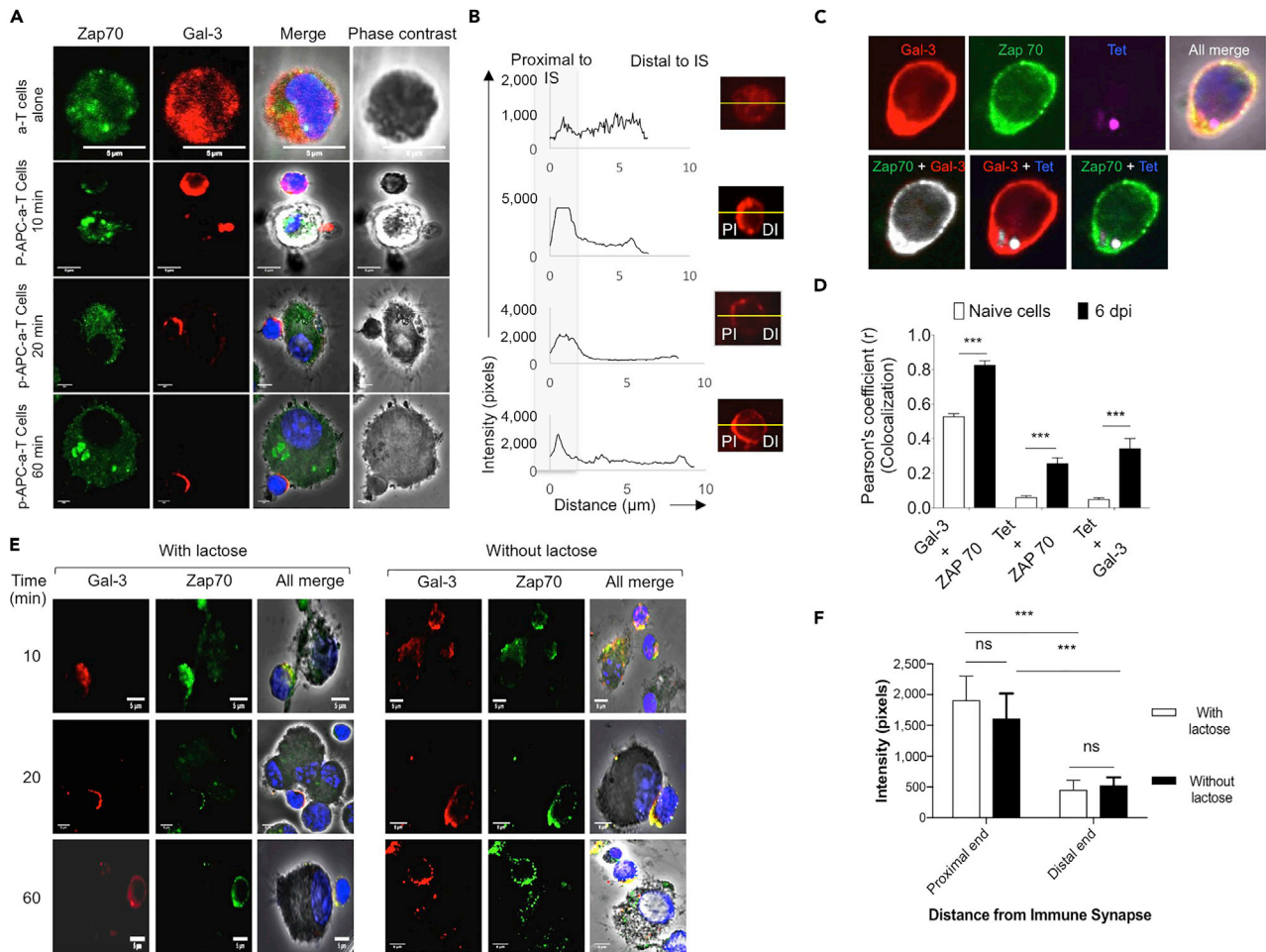
Figure 4. Galectin-3 Expressed by Re-stimulated CD8+ T Cells Is Recruited at Immunological Synapse

Magnetically activated cell sorting (MACS)-purified OT1 cells were stimulated *in vitro* using anti-CD3 and anti-CD28 antibodies for 72 hr. Then cells were washed and co-cultured with SIINFEKL-peptide-pulsed BMDCs for indicated time. Thereafter cells were stained for different markers and analyzed by confocal microscopy for distribution of galectin-3.

(A) Micrographs show the expression of different molecules and their migration toward immunological synapse involving activated OT1T cells and BMDCs at different time post stimulation.

(B) The intensity of galectin-3 expressed in OT1 cells that migrated toward BMDCs is shown. Shaded area represents intensity of fluorescent probe proximal to immunological synapse (IS) (PIS) when compared with the intensity observed distal to immunological synapse (DIS).

(C) OT1 cells were transferred in C57BL/6 mice 1 day before the infection with MHV68 M2-SIINFEKL. At 6 days post infection, H-2K^b-SIINFEKL–tetramer-positive cells were FACS sorted and stained for galectin-3 and Zap70. Micrographs show staining of different molecules.

(D) Bar graphs represent co-localization of different molecules in input control cells and OT 1 cells obtained from infected animals at 6 dpi. More than 35 cells were analyzed for each time point. ns, non significant, *** p<0.001.

(E and F) The influence of α-lactose on the recruitment of intracellular versus extracellular galectin-3 at the immunological synapse was analyzed. SIINFEKL-peptide-pulsed BMDCs were co-cultured with OT1 cells FACS sorted from infected animals at 6 dpi in the presence or absence of 100 mM α-lactose solution, and the extent of localization of galectin-3 toward immune synapse was measured. A minimum of 35 cells was counted for each group for calculating co-localization percentages for different molecules. (E) Representative confocal micrographs for the co-localization of galectin-3 and Zap70 are shown. (F) Bar diagram depicting the intensity of galectin-3 at the proximal and distal ends of OT1 cells in contact with peptide-pulsed BMDCs for 35 cellular contacts for each sample is shown. *** p<0.001, ns, non significant.

marrow derived dendritic cells (BMDCs) and stained for galectin-3 and Zap70. Cells not re-stimulated with peptide-pulsed BMDCs exhibited diffuse staining for galectin-3 (Figure 4A, upper panel). Within 10 min of co-culture with peptide-pulsed BMDCs, galectin-3 localized toward the immune synapse and remained so until 60 min; Figure 4A lower three panels and Figure 4B). In these experiments, we did not observe enhanced expression and recruitment of Zap70 to the synapse in re-stimulated cells. CD8+ T cells become temporarily refractory to re-stimulation as the TCR (Demotte et al., 2008). We also performed

co-localization experiments using CD8^{+} T cells that were expanded as a result of viral infections and isolated in the acute phase of response at 6 dpi (Figures S5A–S5C). Galectin-3 was upregulated in antigen-specific CD8^{+} T cells responding to invading viral infections. We used two different viruses (a γ-HV [MHV68] and an influenza virus) to investigate galectin-3 expression and localization in reactive CD8^{+} T cells (Figures 4C, 4D, S5, and S6). Activated cells were then stained to assess co-localization of galectin-3 with class I MHC tetramers and Zap70. Staining of CD8^{+} T cells with class I MHC tetramers marked the expression of TCR. We observed significant co-localization of galectin-3 with MHC tetramers (∼40%) and Zap70 (more than 80%). In addition, Zap70 and class I MHC tetramers also exhibited a co-localization to the extent of 40% (Figures 4C and 4D). Therefore, our results show that galectin-3 is recruited at the immune synapse during activation of CD8^{+} T cells.

While analyzing co-localization of galectin-3 at immune synapse, we added α-lactose to the co-culture of activated OT1 cells and SIINFEKL-pulsed BMDCs to determine whether or not CD8^{+} T cells produced galectin-3 acts intracellularly or extracellularly. α-Lactose inhibits interaction between CRD of galectins and carbohydrate moieties present on other proteins (Demetriou et al., 2001). Addition of α-lactose, which is likely to act extracellularly by competing with galectins for binding to glycosylated proteins, did not alter the expression kinetics and recruitment of galectin-3 or Zap70 toward the proximal end of the immune synapse (Figures 4E and 4F). Whether or not α-lactose treatment of cells during their activation influences the activation of CD8^{+} T cells was also measured cytofluorometrically 12 hr post stimulation with plate-bound anti-CD3 and soluble CD28 antibodies (Figure S4E). CD8^{+} T cells stimulated in the presence of α-lactose displayed an impaired activation profile as measured by CD69 staining (Figure S4E). α-Lactose may act not only to compete with galectin-3 but also to other galectins. Therefore, we investigated the influence of extracellular galectin-3 neutralization by specific antibody clone (B2C10) that was previously shown to bind extracellular galectin-3 (Gordon-Alonso et al., 2017; Yip et al., 2017). We also performed experiments using this clone to validate its ability to bind cell surface as well as extracellular galectin-3 (Figure S4F). As naive and activated CD8^{+} T cells did not display significant amount of galectin-3 on their surface (Figure S4D), we reasoned that the primary immune cells other than those expressing CD8 molecule might be used to demonstrate its surface detection. Splenocytes as well as lymph node cells did not express galectin-3 on their surface, but about 25% of total splenocytes and 12% of lymph node cells that were CD8 negative show its surface expression (Figure S4F). In addition, we performed galectin-3 pull-down experiments using B2C10 clone of anti-galectin-3, which will demonstrate its ability to bind a soluble extracellular galectin-3. The results shown in Figure S4G demonstrate that a polypeptide of about 30 kDa, the molecular mass of galectin-3, was specifically bound by anti-galectin-3 antibody. The result of surface galectin-3 neutralization experiments using anti-galectin-3 antibodies are described in a later sections.

Long-term protective immunity to intracellular infections or vaccines is critically dependent on memory response. Therefore, we investigated whether or not galectin-3 is also involved in regulating the immune synapse formation by virtue of its localization at proximal end during the activation of memory CD8^{+} T cells. We infected OT1-cell-recipient mice with MHV68-SIINFEKL and analyzed CD8^{+} T cells in the memory stage (55 dpi) by flow cytometry and confocal microscopy (Figure 5A). All H-2K[b]-SIINFEKL-specific CD8^{+} T cells expressed high level of CD44 (CD44^{hi}) but low level of CD62L (CD62L^{lo}) and IL-7R (IL-7R^{lo}) (Figure 5B). This phenotype was previously reported during a persistent γ-HV (MHV68) infection (Jennings et al., 2014). Galectin-3 co-localized with Zap70 and tetramers to the extent of ∼80% and ∼40%, respectively (Figures 5C and 5D), whereas co-localization of Zap70 with tetramers was ∼30% in stimulated H-2K[b] SIINFEKL-specific cells with immobilized tetramers. Therefore, similar to what was observed during the initial activation of naive CD8^{+} T cells after MHV68 infection, the stimulation of specific memory CD8^{+} T cells exhibited galectin-3 recruitment at the immune synapse.

The phenotype of memory CD8^{+} T cells generated during a persistent infection is distinct from that generated during an acute viral infection. We therefore analyzed memory cells generated during an acute infection with influenza virus. We infected mice with an influenza virus encoding a SIINFEKL epitope (WSN-SIINFEKL) and analyzed endogenous antigen-specific memory CD8^{+} T cells at 40 dpi (Figure 5E). Infected mice demonstrated a transient drop in body weight (Figure S5B). H-2K[b]-SIINFEKL-specific CD8^{+} T cells isolated in the acute phase of response demonstrated a high expression of activation marker CD44 and KLRG1 (Figure S5C). When analyzed during memory stage after 40 dpi, H-2K[b]-SIINFEKL-specific CD8^{+} T cells were heterogeneously stained for CD44, CD62L, and IL-7R, a phenotype distinct from those of memory cells generated during persistent MHV68 infection (Figure 5F). Sorted H-2K[b]-SIINFEKL-specific CD8^{+} T cells during the acute (Figure S5D) as well as memory stage (Figures 5G and 5H) of infection
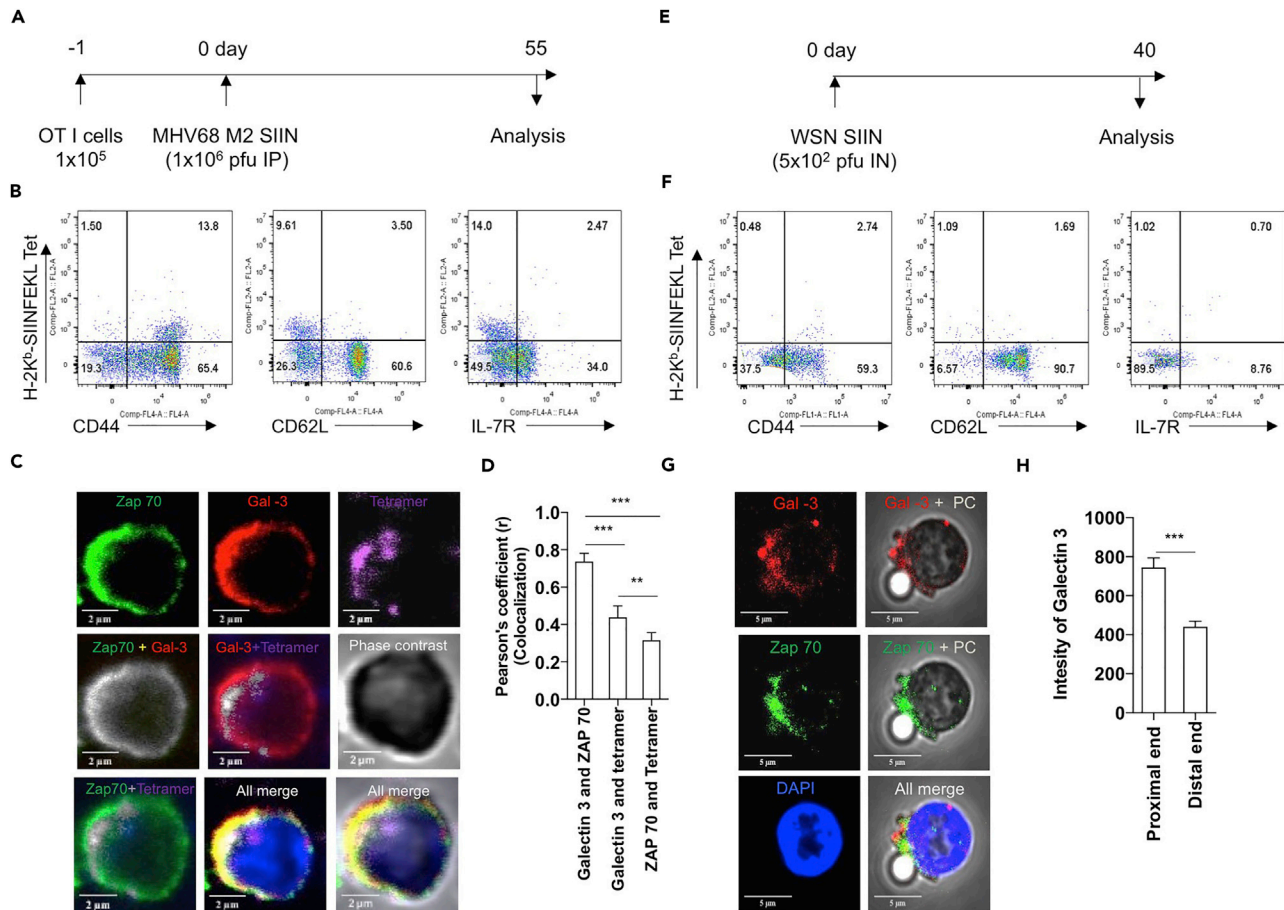
Figure 5. Galectin-3 Expressed by Memory Cells Generated during γ-HV (MHV-68 M2SIINFEKL) and Influenza Virus (WSN-SIINFEKL) during Their Recall Response Is Recruited at Immunological Synapse

(A) 1×10^5 OT1 cells were adoptively transferred in C57BL/6 mice 1 day before infection with MHV68-M2SIINFEKL virus.

(B) Phenotypic characterization of H-2K^b-SIINFEKL-specific CD8 T cells was performed flow cytometrically. Representative FACS plots are shown.

(C and D) H-2K^b-SIINFEKL-specific CD8 T cells were FCAS purified at 55 dpi and stimulated by H-2K^b-SIINFEKL tetramer coated on coverslips for 1 hr. Thereafter cells were stained for different markers and analyzed by confocal microscopy for distribution of galectin-3. (C) Representative confocal micrographs show the expression of different molecules. (D) Bar graphs represent co-localization of different molecules in H-2K^b-SIINFEKL cells. More than 30 cells were analyzed. **$p<0.01$ and ***$p <0.001$.

(E–H) (E) C57BL/6 mice were infected with WSN-SIINFEKL, and endogenous H-2K^b-SIINFEKL-specific cells purified at 40 dpi by H-2K^b-SIINFEKL-monomer-coated magnetic beads were analyzed by flow cytometry and confocal microscopy. (F) Phenotypic characterization of endogenous H-2K^b-SIINFEKL-specific CD8$^+$ T cells was performed flow cytometrically. Representative FACS plots are shown. (G) Representative confocal micrographs show the expression and co-localization of different molecules. (H) Bar diagram shows the intensity (pixels) of galectin-3 at the proximal and distal ends of specific cells and H-2K^b-monomer-coated bead contacts. At least 30 such contacts were counted. ** p value < 0.01 and *** p value < 0.001.

were analyzed for recruitment of galectin-3 at the immune synapse. As shown in Figures S5D, 5G, and 5H, galectin-3 was recruited alongside Zap70 at the synapse formed between SIINFEKL-specific CD8$^+$ T cells and H-2K^b-SIINFEKL-coated beads.

Taken together, our results demonstrate that galectin-3 is upregulated in antigen-specific CD8$^+$ T cells upon MHV68 as well as influenza virus infection and is recruited to the immunological synapse during their primary as well as memory stimulation.

Galectin-3 Regulates Proliferation and Cytokine Production by CD8$^+$ T Cells

Having established that galectin-3 is recruited to the immunological synapse in CD8$^+$ T cells after stimulation, we investigated whether extracellular galectin-3 neutralization improves activation and cytokine production by CD8$^+$ T cells *in vitro*. We stimulated purified Carboxyfluorescein succinimidyl ester
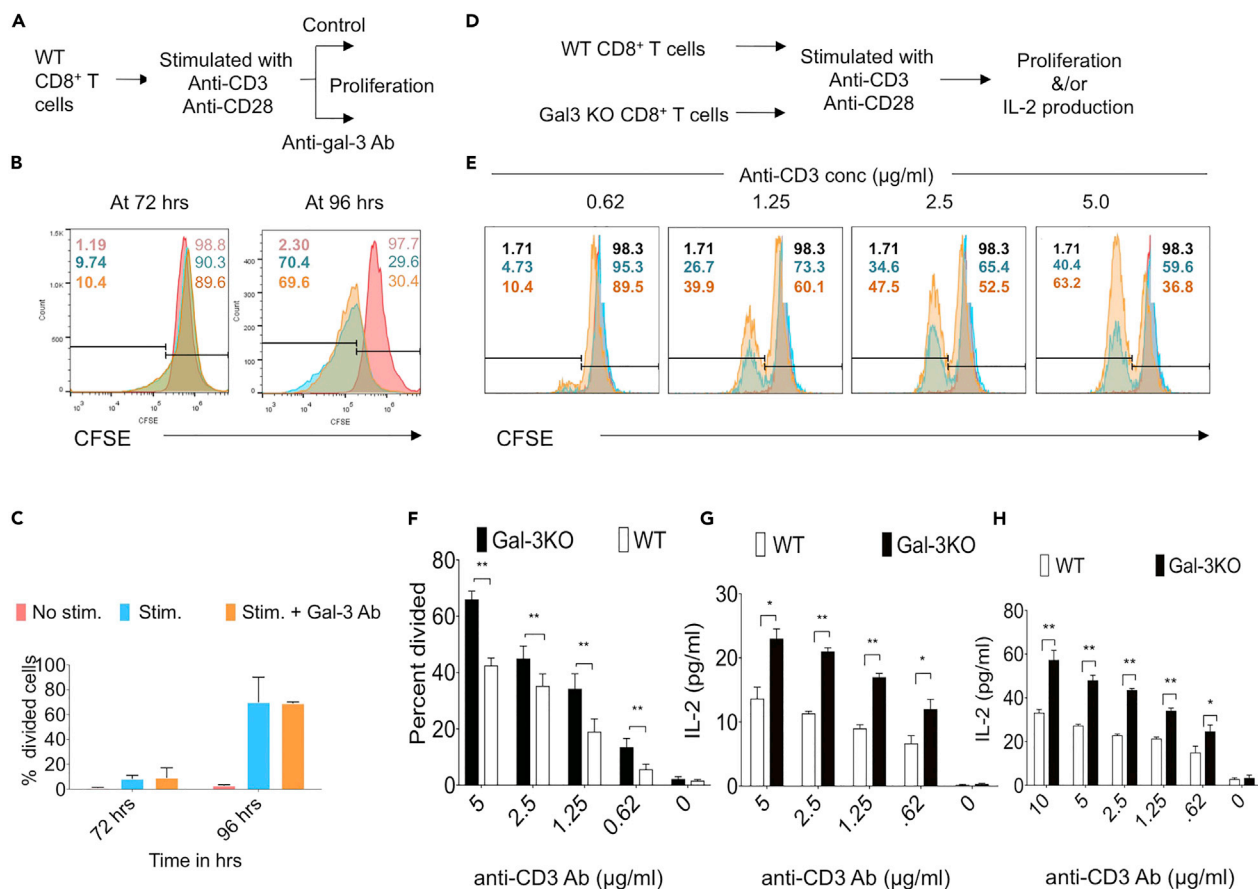
Figure 6. Cell-Autonomous Intracellular Expression of Galectin-3 in CD8+ T Cells Is Responsible for Regulating Their Proliferation and Cytokine Production

(A) A schematic of the experiment to investigate influence of galectin-3 in anti-MHV68 specific CD8+ T cell responses. Purified CD8+ T cells labeled with CFSE were stimulated with plate bound anti-CD3 (1μg/ml) and soluble anti-CD28 (1μg/ml) antibodies in the presence or absence of neutralizing anti-galectin-3 (10μg/ml) antibody. The proliferation was measured by CFSE dilution.

(B) Representative overlaid histograms show the proliferation of CD8+ T cells in the presence or absence of anti-galectin-3 antibody. The numbers written in bold fonts represent the numbers of divided cells in unstimulated cells (reddish), stimulated cells (blue) and stimulated cells added with anti-galectin-3 antibody (orange).

(C) Bar diagram show the percentage of divided cells at 72 hrs and 96 hours in CD8+ T cells stimulated in the presence or absence of anti-galectin-3 antibody. Addition of neutralizing gal-3 antibody did not alter the proportion of divided cells. D-H. An influence of galectin-3 in causing CD8+ T cell activation was measured using gal-3 KO T cells.

(D) A schematic of the experiment is shown. CD8+ T cells were MACS purified from WT and galectin-3 KO mice and labeled with CFSE. Labeled cells were then stimulated in vitro with indicated concentration of soluble anti-CD3 and 1μg/ml of anti-CD28. Dilution of CFSE in CD8+ T cells was measured cytofluorimetrically and IL-2 levels were measured in the culture supernatants by sandwich ELISA.

(E) Histograms show the proliferation of WT and galectin-3 deficient CD8+ T cells at indicated concentrations of anti-CD3. The numbers written represent the proportion of divided cells (on left side) and undivided cells (right side of histograms) in un-stimulated (black), WT (blue) and galectin-3 deficient CD8+ T cells (orange).

(F) Bar diagram show the percentage of divided cells from galectin-3 KO and WT animals when stimulated with indicated concentrations of anti-CD3. **p < 0.01.

(G) Bar diagrams show IL-2 levels in the culture supernatants of WT and galectin-3 deficient CD8 T cells. * p < 0.05, **p < 0.01.

(H) Total splenocytes isolated from WT and galectin-3 KO animals were stimulated with indicated concentrations of anti-CD3 and 1μg/ml of anti-CD28 for 60 hours and IL-2 levels were measured by ELISA. Bar diagrams show the levels (mean ±SD) of IL-2 for three separate wells in WT and galectin-3 KO animals at indicated concentration of anti-CD3. *p < 0.05, **p < 0.01. The experiments were repeated three times with similar results.

(CFSE)-labeled CD8+ T cells with anti-CD3 and soluble anti-CD28 antibodies in the presence or absence of a neutralizing anti-galectin-3 antibody (Figure 6A). In the absence of antibody treatment, approximately 10% and 70% of CD8+ T cells divided at 72 and 96 hr post stimulation, respectively, upon incubation with anti-CD3 (1 μg/mL of plate-bound) and soluble anti-CD28 antibodies (Figures 6B and 6C). Extracellular

galectin-3 neutralization with neutralizing antibody did not affect the proportion of divided cells as measured by CFSE dilution assays at 72 and 96 hr post stimulation (Figures 6B and 6C).

To further investigate a cell-autonomous contribution of galectin-3 in activating CD8^{+} T cells, we magnetically isolated CD8^{+} T cells from WT and galectin-3 KO mice and stimulated equal numbers of CFSE-labeled CD8^{+} T cells, by application of different concentrations of anti-CD3 and soluble anti-CD28 (1 μg/mL) antibodies. We measured CFSE dilution as an indicator of proliferation and IL-2 production in culture supernatants as an indicator of their functionality (Figure 6D). More CD8^{+} T cells from galectin-3 KO mice proliferated than those from WT mice at all concentrations of anti-CD3 antibody tested (Figures 6E and 6F). Galectin-3-deficient CD8^{+} T cells produced more IL-2 than WT CD8^{+} T cells in response to anti-CD3/anti-CD28 antibody treatment (Figure 6G). We also stimulated splenocytes from galectin-3 KO and WT mice with anti-CD3/anti-CD28 antibodies and measured their proliferation and cytokine production. Similar to the response of CD8^{+} T cell, total T cells, which also included responding CD4^{+} T cells from galectin-3 KO mice, produced more IL-2 than their WT counterparts (Figure 6H).

A deficiency of galectin-3 in T cells is therefore responsible for their enhanced proliferation and cytokine production, and galectin-3 could predominantly act in a cell-autonomous manner and intracellularly to inhibit T cell functions.

Galectin-3 Deficiency Enhances MHV68-Specific CD8^{+} T Cell Response

After demonstrating a regulatory intracellular function of galectin-3 during the immunological synapse formation, we explored whether a loss of galectin-3 expression has functional consequences in modulating a virus-specific CD8^{+} T cell response. We infected WT and galectin-3 KO mice with MHV68 (Figure 7A) and measured the magnitude of virus-specific CD8^{+} T cells isolated from spleens by MHC tetramer staining and ICCS assays. Galectin-3 KO animals mounted a stronger virus-specific CD8^{+} T cell response than WT animals (Figures 7B–7E). Using MHC tetramers, we investigated recognition of CD8^{+} T cell epitopes derived from five different ORFs of MHV68. Both early (ORF9 and ORF75c) and late (ORF6, ORF8, ORF17, and ORF61) MHV68 antigens were examined (Freeman et al., 2010; Gredmark-Russ et al., 2008). Galectin-3 KO mice showed greater expansion of their virus-specific CD8^{+} T cells than WT mice (Figures 7B and 7C). Intracellular cytokine assays were performed to measure IFN-γ-producing cells in response to H-2K[b]- and H-2D[b]-restricted peptides. The frequencies of cytokine-producing splenic CD8^{+} T cells were significantly higher for most of the epitopes for galectin-3 KO animals than those for WT animals (Figures 7D and 7E). ORF61- and ORF75c-reactive CD8^{+} T cells expanded to a greater extent than those recognizing other ORFs (Figure 7). CD8^{+} T cells that recognize ORF61, a ribonucleotide reductase, may be critically involved in the maintenance of viral latency (Freeman et al., 2010; Gredmark-Russ et al., 2008). ORF75c, a tegument protein of MHV68, exhibits ubiquitin E3 ligase activity and can target degradation of promyelocytic leukemia, essential for the pathogenesis of γ-HV-induced transformation and in modulating apoptosis (Ling et al., 2008). An ORF75c-null virus is compromised in its ability to establish latency as well (Gaspar et al., 2008). Thus, enhancing the frequency of CD8^{+} T cells specific for ORF75c and ORF61 may be a means of interfering with γ-HV-mediated pathogenesis. Lack of galectin-3 signaling in virus-specific CD8^{+} T cells by enhancing their responsiveness could perhaps improve protection against this γ-HV.

Enhanced MHV68-Specific CD8^{+} T Cell Response Leads to More Efficient Viral Control in Galectin-3 KO Mice

We asked whether or not a stronger anti-viral CD8^{+} T cell response in galectin-3 KO mice would help control the virus more efficiently than in WT mice. Galectin-3 KO and WT animals were infected intranasally with MHV68 so that we could measure replicating virus in lung tissues. The functionality of anti-viral CD8^{+} T cells and viral titers in lung tissues of infected animals were then measured (Figure 8A). We measured the frequencies of activated CD8^{+} T cells, i.e., TIM-3^{+}, CD44^{+}, and TIM-3^{+}CD44^{+} CD8^{+} T cells, in the mediastinal lymph nodes of MHV68-infected galectin-3 KO and WT mice (Figures 8B–8E). TIM-3 expression on CD8^{+} T cells marks antigen-experienced cells (Sehrawat et al., 2010). More TIM-3^{+}CD8^{+} T cells were present in the lymph node (LN) of galectin-3 KO animals (10.6%) than in WT animals (4.6%) (Figures 8B–8E). Only a subset CD44^{hi}CD8^{+} T cells expressed TIM-3 (Figure 8C). Galectin-3 KO animals also had more activated CD8^{+} T cells (CD44^{hi} CD8^{+}: 18% in WT and 31% in galectin-3 KO mice) (Figures 8D and 8E). The frequencies of IFN-γ-positive CD8^{+} T cells isolated from MLN were measured by ICCS assays in response to known MHV68-specific CD8^{+} T cell targets. Seven of these
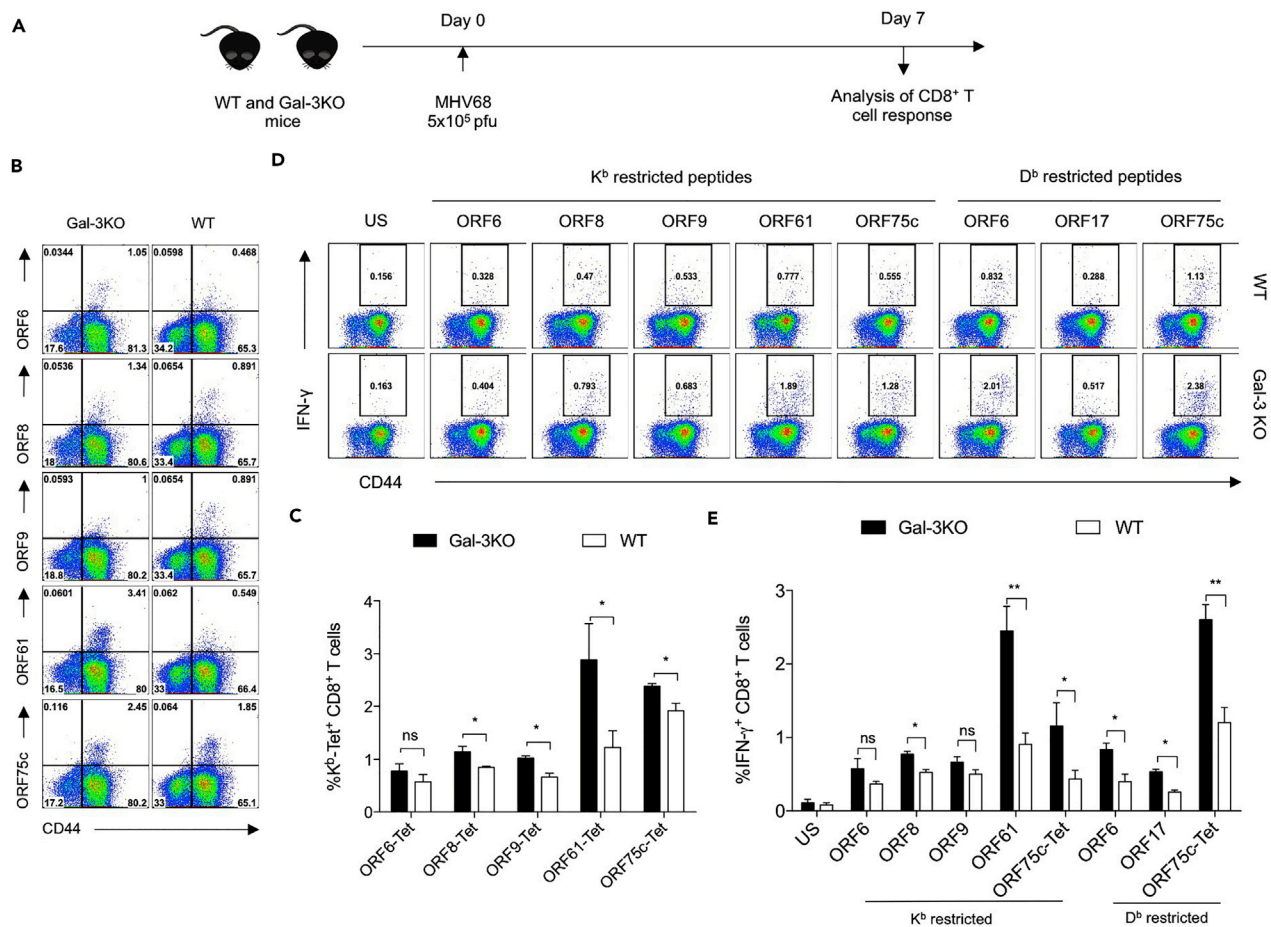
Figure 7. Galectin-3 Deficiency Enhances Magnitudes of γ-HV-specific CD8+ T Cells

(A) A schematic of the experiment to investigate influence of galectin-3 in anti-MHV68-specific CD8+ T cell responses. Galectin-3 KO and C57BL/6 WT mice were i.p. infected with MHV68, and splenocytes were analyzed for surface TCR expression and intracellular cytokine staining.

(B) Representative FACS plots show the frequencies of respective tetramer-specific cells in spleen samples of infected WT and galectin-3 KO mice. Tetramers for respective ORFs were generated using a UV-mediated photocleavage reaction, and the exchange was performed to displace conditional ligand with peptide sequences derived from the indicated ORFs of MHV68.

(C) Bar diagrams show the frequencies of respective peptide-specific CD8+ T cells measured from at least four different animals per group. The experiments were repeated at least two times with similar results.

(D) Representative FACS plots show IFN-γ-producing CD8+ T cells measured using ICCS assays. Splenocytes from WT and galectin-3 KO animals were stimulated with peptides derived from indicated ORFs of MHV68, and the cells were analyzed using flow cytometry.

(E) Bar diagrams show the frequencies (mean ± SD) of IFN-γ-producing cells reactive to class I MHC epitopes of indicated ORF-derived peptides measured for four WT and galectin-3 KO animals per group.

eight peptides evoked significantly more IFN-γ-positive CD8+ T cells in galectin-3 KO animals (Figures 8F and 8G). This was true for both H-2K^b- and H-2D^b-restricted epitopes. Viral titers were measured in lung tissues of galectin-3 KO and WT mice and showed up to a 100-fold reduction in galectin-3 KO mice on 6 dpi (Figure 8H). Similar results were obtained when viral titers were measured at different time points (data not shown).

Galectin-3 Contributed by Cells Other Than CD8+ T Cells Does Not Affect Virus-Induced Expansion of Specific CD8+ T Cells

Many cell types, including T cell, B cells, myeloid cells, and stromal cells may produce galectin-3 (Hsu et al., 2009). We investigated whether or not galectin-3 contributed by cells other than CD8+ T cells affects the expansion of virus-specific CD8+ T cells. We transferred 50 × 10³ ORF8 TCR TN CD8+ T cells into WT and galectin-3 KO mice 1 day before MHV68 infection and measured the frequencies of expanded cells 7 days later (Figure 9A). Both endogenous and transferred ORF8-specific TN cells were analyzed. The proportion
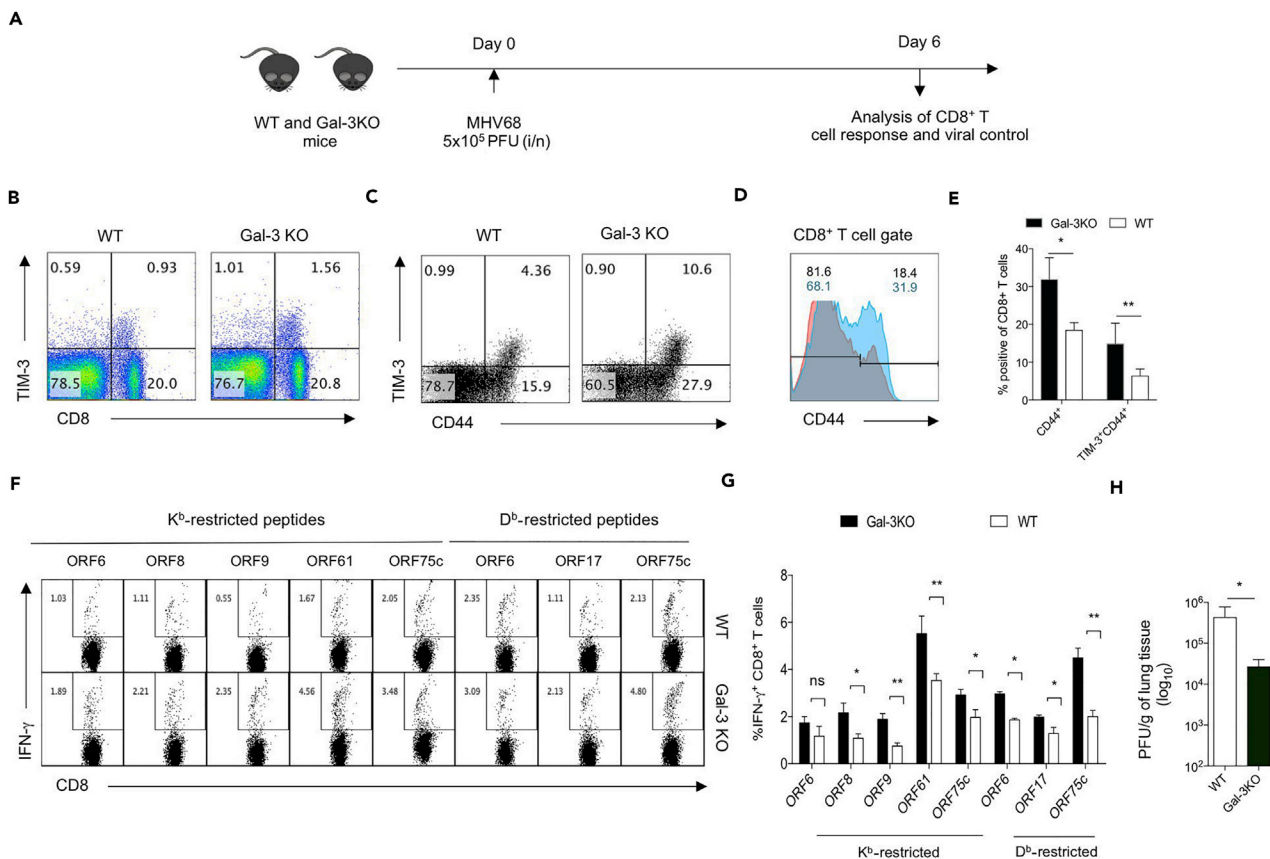
Figure 8. Galectin-3-Deficient Animals Efficiently Control γ-HV Infection

(A) A schematic of the experiments is shown. Galectin-3 KO and C57BL/6 WT mice were intranasally infected with 5 × 10⁵ plaque-forming unit (PFU) of MHV68. Mediastinal lymph nodes were analyzed at 6 dpi by surface staining and intracellular cytokine staining for measuring the phenotype and functions of CD8⁺ T cells. Lungs were collected from the infected animals, and the viral titers were measured.

(B) Representative FACS plots show the frequencies of TIM-3⁺-activated CD8⁺ T cells in live cell gate isolated from the lymph nodes of WT and galectin-3 KO mice.

(C) FACS plots of CD8⁺ T cell-gated population show the expression of CD44 and TIM-3 in CD8⁺ T cells from WT and galectin-3 KO mice.

(D) Histograms show the expression of CD44 in gated CD8⁺ T cells isolated from lymph nodes of WT and galectin-3 knockout mice. Numbers in overlaid histograms represent proportion of CD44^{lo} and CD44^{hi} populations of WT (regular font) and galectin-3 knockout (bold font).

(E) Bar diagrams show the percentage of CD44⁺ and CD44⁺TIM-3⁺ CD8⁺ T cells in WT and galectin-3 KO animals. *p<0.05, **p <0.01.

(F) FACS plots show the frequencies of IFN-γ-positive cells in response to different MHC class I (H-2K^b and H-2D^b-restricted) epitopes derived from ORFs of MHV68.

(G) Bar diagrams showing the frequencies (mean ± SD) of IFN-γ-producing CD8⁺ T cells from a representative experiment in which four WT and four galectin-3 KO animals were used. ns, non significant, * p< 0.05, ** p< 0.01.

(H) Bar diagram shows virus titers in the lungs of the four animals each from WT and galectin-3 KO group at 6 dpi. The experiments were repeated two times with similar results. *p <0.05.

of activated and expanded ORF8 TCR TN CD8⁺ T cells was similar in both the galectin-3 KO and WT animals (Figures 9B and 9C), suggesting a negligible effect of exogenous galectin-3 in the magnitude of γ-HV-specific CD8⁺ T cells. Galectin-3 deficiency therefore may exert a cell-autonomous phenotype in CD8⁺ T cells expanded during MHV68 infection.

DISCUSSION

γ-HVs are species-specific pathogens. An investigation of their pathogenesis thus requires a natural host as the relevant animal model. An understanding of host correlates of protection to γ-HVs is confounded by the likelihood that these may show host-specific elements as well. Consequently, strategies for vaccine development have suffered due to the absence of reliable animal models. MHV68 infection of mice offers one such model system to study the immunity and immunopathology to γ-HVs (Barton et al., 2011). We
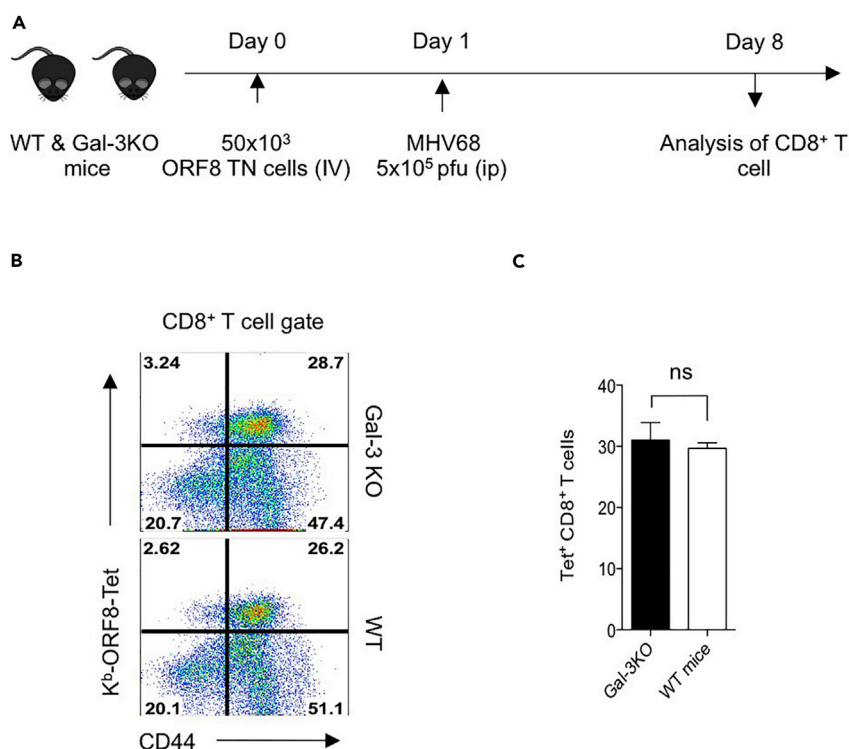
Figure 9. Expansion of Virus-Specific CD8+ T Cells during Acute Phase of Infection Is Not Influenced by Exogenous Galectin-3

(A) A schematic of the experiments is shown. 50 × 10³ ORF8 TN cells were adoptively transferred into WT and galectin-3 KO animals, which were then i.p. infected with MHV68. At 6 dpi, the frequencies of ORF8-tetramer-positive cells were analyzed.

(B) Representative FACS plots show the frequencies of Kᵇ-ORF8-tetramer-positive cells in the spleen samples of animals.

(C) Bar diagrams show the frequencies (mean ± SD) of H-2Kᵇ-ORF8 CD8+ T cells obtained from three WT and galectin-3 KO animals. The experiments were repeated two times with similar results. ns, non significant.

generated a CD8+ TCR TN mouse model that serves as a source of homogeneous virus-specific CD8+ T cells, which recognize an epitope derived from membrane glycoprotein B of MHV68 (Sehrawat et al., 2012). We performed RNA-seq on naive and activated MHV68-specific CD8+ TCR TN T cells, the latter isolated in the acute phase of infection, to obtain insights into the molecules and pathways that may be critical to their function. Genes for many transcripts encompassing different biological processes, cellular components, and classes of proteins and of diverse molecular function were differentially expressed. Many of these transcripts have not been reported previously to exhibit a similar expression pattern in the acute phase of other viral infections (Best et al., 2013; Wherry et al., 2007). Further analysis showed that more than 300 transcripts in our dataset were not mapped to the existing Gene Ontology database (Table S5). The transcriptional analysis of endogenous CD8+ T cells is commonly confounded by representation of innumerable TCR affinities, as the analyzed cell population is heterogeneous. The transcriptomic data on differentiating single cell is limited but could provide valuable information. RNA-seq data of differentiating TN CD8+ T cells could provide further insight into their phenotypic and functional attributes. These RNA-seq data could uncover new angles of attack to investigate CD8+ T cell biology. Of course, not only transcription but also the translational status determines the fate of differentiating CD8+ T cells (Araki et al., 2017). Numerous genes differentially expressed in activated TN CD8+ T cells suggest that during differentiation of T cells the translational machinery may be impaired, which could contribute to the contraction of almost 95% of antigen-reactive CD8+ T cells. Manipulation of the translational profile of antigen-stimulated cells could modulate immunological memory and control of infection (Sehrawat et al., unpublished data).

In response to an invading intracellular pathogen, CD8+ T cells expand massively to resolve the infection. Most of the expanded pathogen-specific effector cells are then eliminated during the contraction phase (Ahmed and Gray, 1996). However, mechanisms responsible for their induction, expansion, and elimination

are still not entirely understood and may show considerable heterogeneity, depending on the biology of the pathogen recognized. The role of galectins in the pathogenesis of infection is beginning to be understood (Vasta, 2009). Galectins play a diverse role in immunity upon infection, in autoimmune diseases and cancer (Rabinovich and Toscano, 2009). Through direct interactions with the pathogen or by modulating the microenvironment in which pathogens reside, galectins can either promote or prevent viral infections (Vasta, 2009). For example, galectin-1 could promote HIV infection of macrophages by directly binding to its surface glycoproteins and serving as a bridge between the virus and immune cells (Mercier et al., 2008; Ouellet et al., 2005). Galectins can also help attract susceptible immune cells to sites of infection (Sano et al., 2000). Viruses such as HIV, EBV, Nipah virus, and HV 1 modulate the expression of various galectins in host cells (Vasta, 2009). One could therefore argue that galectin-3 deficiency might interfere with a productive replication of γ-HVs such that the overall antigen levels are reduced. We observed enhanced antiviral CD8$^+$ T cell immunity in galectin-3 KO mice, which could represent an underestimation rather than an overestimation of antigen-specific CD8$^+$ T cells. Galectin 3-deficient animals mounted a stronger anti-MHV68 CD8$^+$ T cell response to seven of eight epitopes, regardless of whether restricted by H-2K^b or H-2D^b, thus improving virus control. Similarly an enhanced expansion and cytokine production by co-receptor-stimulated CD8$^+$ T cells was observed.

During activation of CD8$^+$ T cells, actin microfilaments help coalesce the glycoproteins involved in the formation of immunological synapse (Dustin and Cooper, 2000). Our RNA-seq data showed upregulation of two members of the galectin family, i.e., galectin-3 (up ~140-fold) and galectin-1 (up ~87-fold), in activated TN CD8$^+$ T cells during the acute phase of infection with MHV68. Galectin-3 has one CRD but exhibits a greater tendency to multimerize upon binding to glycoconjugates than other galectins (Lepur et al., 2012). This effect is attributed to its non-lectin N-terminal domain, which is rich in proline and glycine residues (Menon and Hughes, 1999). Exposure of T cells to exogenous galectin-3 might cause their apoptosis, whereas endogenous expression of galectin-3 was found to exert an anti-apoptotic function (Fukumori et al., 2004). However, another study showed that activated CD8$^+$ T cells as a result of herpes simplex virus 1 did not undergo apoptosis upon treatment with exogenous galectin-3 (Sehrawat et al., 2010). Therefore, the influence of galectin-3 on immune cells could be context dependent.

Galectin-3 is recruited to the immunological synapse during activation of CD4$^+$ T cell response (Chen et al., 2009). In view of its upregulation in MHV68-specific TCR TN CD8$^+$ T cells, we investigated whether galectin-3 expression has a functional consequences in resolving the infection. We find that galectin-3 expression was upregulated at the transcriptional and at a protein product level upon viral infections as well in co-receptor-stimulated CD8$^+$ T cells within 16 hr, and the expression further increased on 3 days post stimulation (Figure 2). This was true for MHV68- as well as influenza-virus-expanded antigen-specific CD8$^+$ T cells, thereby attesting to the fact that pathogen-specific elements and their interaction by host could play a role in fine-tuning T cell responses (Figures 5 and S5). The milieu generated during some chronic infection is enriched in inhibitory cytokines such as IL-10, which could promote the activity of glycosyltransferases such as Mgat5, which in turn promoted the modification of N-linked glycans for various surface proteins (Smith et al., 2018). Galectin-3 might interfere with the recruitment of such proteins during activation of T cells, thereby increasing the threshold of TCR signaling. This effect may be predominantly extracellular in nature. Our investigation focusing on intracellular versus extracellular involvement of galectin-3 in shaping T cell responses against γ-HVs revealed predominantly an intracellular role of this molecule as the neutralization of extracellular galectin-3 either by α-lactose or by anti-galectin-3 antibody did not seem to influence the recruitment of galectin-3 to immune synapse or the proliferation of stimulated cells (Figures 4 and 6). The α-lactose treatment could also interfere with the activity of other galectins, which was also reflected in experiments investigating its role in the activation of T cells. Accordingly, in some experiments in which α-lactose was added during the activation of CD8$^+$ T cells their activation was impaired, which might suggest the role of other players (Figure S4E). Therefore, the experiments aimed at the neutralization of galectin-3 function by an antibody provided more relevant information with respect to its intracellular versus extracellular role in cellular activation (Figures 6A–6C). That the antibody used could affect extracellular galectin-3 neutralization was shown earlier (Gordon-Alonso et al., 2017; Yip et al., 2017). Our experiments also demonstrate the binding of the antibody to extracellular galectin-3 (Figures S4F and S4G).

We observed that upon their co-culture with cognate-peptide-pulsed APCs, galectin-3 rapidly recruited to the immunological synapse in CD8$^+$ T cells undergoing a primary as well as a secondary stimulation (Figures 3, 4, and 5). Expression of galectin-3 compromised the magnitude of virus-specific CD8$^+$ T cells to clear

the virus, as galectin-3-deficient CD8^{+} T cells showed an enhanced frequency for almost all epitopes of MHV68. The ability of galectin-3 to constrain anti-viral immunity is counterintuitive, but its presence at the immunological synapse could help attenuate spontaneous activation of the TCR to avoid immunopathological reactions, particularly to self-antigens (Radosavljevic et al., 2012). Development and maintenance of peripheral CD8^{+} T cells requires sustained low-affinity interactions that involve self-peptides loaded onto MHC I molecules (Ziegler et al., 2009). Therefore, the presence of galectin-3 at synapse could act as a break to constrain any possible hyperactivity. Galectin-3 is also thought to compromise the activity of cytotoxic CD8^{+} T cells during some autoimmune diseases as well as in the tumor microenvironment (Fortuna-Costa et al., 2014; Kouo et al., 2015; Nangia-Makker et al., 2008). In a tumor environment the interaction of galectin-3 with T cells effector cytokine IFN-γ compromised its protective function, and the effect is extracellular in nature. However, how galectin-3 acts to constrain anti-viral CD8^{+} T cell immunity during HV infection is still not understood and was elucidated in this study. We found that galectin-3 contributed by cells other than CD8^{+} T cells had little influence in impairing the induction, activation, and expansion of MHV68- specific TN CD8^{+} T cells *in vivo* (Figure 9). The role of galectin-3 in CD8^{+} T cells during a γ-HV infection is thus cell autonomous.

The distribution of single-positive CD4^{+} and CD8^{+} T cells in the thymus of galectin-3 KO and WT animals were similar, suggesting that during development of these cells galectin-3 may not be playing a major role and predominantly regulates reactivity of T cells in the periphery (Figure S7). The observation that memory CD8^{+} T cells when recalled by antigenic stimulation does induce the recruitment of regulatory galectin-3 to immune synapse can have implication in designing the regimen for priming and boosting vaccine-specific CD8^{+} T cell immunity. Our results suggest that modifying galectin-3 function in CD8^{+} T cells and not in a generic manner could be considered as a strategy to enhance anti-viral CD8^{+} T cell immunity, for example, through the disruption of its localization to the immune synapse by using small molecules or intrabodies, by manipulation of its glycosylation status, or even by adjusting the expression levels of galectin-3 itself.

Limitation of Study

The aim of this study was to investigate the role of galectin-3 in influencing anti-γ-HV immunity; an extensive kinetics of T cells activation and differentiation in an environment lacking in galectin-3 versus the one sufficient for its response was not investigated and constitutes part of our ongoing investigations.

METHODS

All methods can be found in the accompanying Transparent Methods supplemental file.

SUPPLEMENTAL INFORMATION

Supplemental Information includes Transparent Methods, seven figures, and five tables and can be found with this article online at https://doi.org/10.1016/j.isci.2018.10.013.

AUTHOR CONTRIBUTIONS

S. Sehrawat and H.L.P. conceived the study. M.K. and S. Sehrawat designed and performed experiments. S. Sehrawat, M.K., and S. Singh analyzed the data. D.K. produced critical reagents for experiments. S. Sehrawat, V.B., and S. Singh analyzed the transcriptomic data. M.K., S. Sehrawat and H.L.P. wrote and edited the manuscript. H.L.P., A.E., and G.R.F. contributed to reagents and animals.

DECLARATION OF INTERESTS

The authors declare no competing interests.

REFERENCES

Ahmed, R., and Gray, D. (1996). Immunological memory and protective immunity: understanding their relation. Science 272, 54–60.

Amanna, I.J., Slifka, M.K., and Crotty, S. (2006). Immunity and immunological memory following smallpox vaccination. Immunol. Rev. 211, 320–337.

Araki, K., Morita, M., Bederman, A.G., Konieczny, B.T., Kissick, H.T., Sonenberg, N., and Ahmed, R. (2017). Translation is actively regulated during the differentiation of CD8+ effector T cells. Nat. Immunol. 18, 1046–1057.

Barton, E., Mandal, P., and Speck, S.H. (2011). Pathogenesis and host control of gammaherpesviruses: lessons from the mouse. Annu. Rev. Immunol. 29, 351–397.

Best, J.A., Blair, D.A., Knell, J., Yang, E., Mayya, V., Doedens, A., Dustin, M.L., and Goldrath, A.W.; Immunological Genome Project Consortium (2013). Transcriptional insights into the CD8(+) T cell response to infection and memory T cell formation. Nat. Immunol. 14, 404–412.

Böhmer, C., Bröer, A., Munzinger, M., Kowalczuk, S., Rasko, J.E.J., Lang, F., and Bröer, S. (2005). Characterization of mouse amino acid transporter B0AT1 (slc6a19). Biochem. J. 389, 745–751.

Chen, H.-Y., Fermin, A., Vardhana, S., Weng, I.-C., Lo, K.F.R., Chang, E.-Y., Maverakis, E., Yang, R.-Y., Hsu, D.K., Dustin, M.L., et al. (2009). Galectin-3 negatively regulates TCR-mediated CD4+ T-cell activation at the immunological synapse. Proc. Natl. Acad. Sci. U S A 106, 14496–14501.

Demetriou, M., Granovsky, M., Quaggin, S., and Dennis, J.W. (2001). Negative regulation of T-cell activation and autoimmunity by Mgat5 N-glycosylation. Nature 409, 733–739.

Demotte, N., Stroobant, V., Courtoy, P.J., Van Der Smissen, P., Colau, D., Luescher, I.F., Hivroz, C., Nicaise, J., Squifflet, J.-L., Mourad, M., et al. (2008). Restoring the association of the T cell receptor with CD8 reverses anergy in human tumor-infiltrating lymphocytes. Immunity 28, 414–424.

Donato, R., Cannon, B.R., Sorci, G., Riuzzi, F., Hsu, K., Weber, D.J., and Geczy, C.L. (2013). Functions of S100 proteins. Curr. Mol. Med. 13, 24–57.

Dunn, K.W., Kamocka, M.M., and McDonald, J.H. (2011). A practical guide to evaluating colocalization in biological microscopy. Am. J. Physiol. Cell Physiol. 300, C723–C742.

Dustin, M.L., and Cooper, J.A. (2000). The immunological synapse and the actin cytoskeleton: molecular hardware for T cell signaling. Nat. Immunol. 1, 23–29.

Elliott, A., Leicht, E., Withmore, A., Gesine, E., and Felix, R.-T. (2018). A non parametric significance test for sampled networks. Bioinformatics 34, 64–71.

Fooksman, D.R., Vardhana, S., Vasiliver-Shamis, G., Liese, J., Blair, D.A., Waite, J., Sacristán, C., Victora, G.D., Zanin-Zhorov, A., and Dustin, M.L. (2010). Functional anatomy of T cell activation and synapse formation. Annu. Rev. Immunol. 28, 79–105.

Fortuna-Costa, A., Gomes, A.M., Kozlowski, E.O., Stelling, M.P., and Pavão, M.S.G. (2014). Extracellular galectin-3 in tumor progression and metastasis. Front. Oncol. 4, 138.

Freeman, M.L., Lanzer, K.G., Cookenham, T., Peters, B., Sidney, J., Wu, T.-T., Sun, R., Woodland, D.L., Sette, A., and Blackman, M.A. (2010). Two kinetic patterns of epitope-specific CD8 T-cell responses following murine gammaherpesvirus 68 infection. J. Virol. 84, 2881–2892.

Fukumori, T., Takenaka, Y., Oka, N., Yoshii, T., Hogan, V., Inohara, H., Kanayama, H., Kim, H.-R.C., and Raz, A. (2004). Endogenous galectin-3 determines the routing of CD95 apoptotic signaling pathways. Cancer Res. 64, 3376–3379.

Gaspar, M., Gill, M.B., Lösing, J.-B., May, J.S., and Stevenson, P.G. (2008). Multiple functions for ORF75c in murid herpesvirus-4 infection. PLoS One 3, e2781.

Gay, O., Gilquin, B., Nakamura, F., Jenkins, Z.A., McCartney, R., Krakow, D., Deshiere, A., Assard, N., Hartwig, J.H., Robertson, S.P., et al. (2011). RefilinB (FAM101B) targets filamin A to organize perinuclear actin networks and regulates nuclear shape. Proc. Natl. Acad. Sci. U S A 108, 11464–11469.

Geserick, P., Kaiser, F., Klemm, U., Kaufmann, S.H.E., and Zerrahn, J. (2004). Modulation of T cell development and activation by novel members of the Schlafen (slfn) gene family harbouring an RNA helicase-like motif. Int. Immunol. 16, 1535–1548.

Gordon-Alonso, M., Hirsch, T., Wildmann, C., and van der Bruggen, P. (2017). Galectin-3 captures interferon-gamma in the tumor matrix reducing chemokine gradient production and T-cell tumor infiltration. Nat. Commun. 8, 793.

Gredmark-Russ, S., Cheung, E.J., Isaacson, M.K., Ploegh, H.L., and Grotenberg, G.M. (2008). The CD8 T-cell response against murine gammaherpesvirus 68 is directed toward a broad repertoire of epitopes from both early and late antigens. J. Virol. 82, 12205–12212.

Hsu, D.K., Chen, H.-Y., and Liu, F.-T. (2009). Galectin-3 regulates T-cell functions. Immunol. Rev. 230, 114–127.

Hughes, R.C. (1999). Secretion of the galectin family of mammalian carbohydrate-binding proteins. Biochim. Biophys. Acta 1473, 172–185.

Jennings, R.N., Grayson, J.M., and Barton, E.S. (2014). Type I interferon signaling enhances CD8+ T cell effector function and differentiation during murine gammaherpesvirus 68 infection. J. Virol. 88, 14040–14049.

Kaech, S.M., and Cui, W. (2012). Transcriptional control of effector and memory CD8+ T cell differentiation. Nat. Rev. Immunol. 12, 749–761.

Kaech, S.M., Tan, J.T., Wherry, E.J., Konieczny, B.T., Surh, C.D., and Ahmed, R. (2003). Selective expression of the interleukin 7 receptor identifies effector CD8 T cells that give rise to long-lived memory cells. Nat. Immunol. 4, 1191–1198.

Kirak, O., Frickel, E.-M., Grotenbreg, G.M., Suh, H., Jaenisch, R., and Ploegh, H.L. (2010). Transnuclear mice with predefined T cell receptor specificities against Toxoplasma gondii obtained via SCNT. Science 328, 243–248.

van Kooyk, Y., and Rabinovich, G.A. (2008). Protein-glycan interactions in the control of innate and adaptive immune responses. Nat. Immunol. 9, 593–601.

Kouo, T., Huang, L., Pucsek, A.B., Cao, M., Solt, S., Armstrong, T., and Jaffee, E. (2015). Galectin-3 shapes antitumor immune responses by suppressing CD8+ T cells via LAG-3 and inhibiting expansion of plasmacytoid dendritic cells. Cancer Immunol. Res. 3, 412–423.

Lepur, A., Salomonsson, E., Nilsson, U.J., and Leffler, H. (2012). Ligand induced galectin-3 protein self-association. J. Biol. Chem. 287, 21751–21756.

Lin, L., Yee, S.W., Kim, R.B., and Giacomini, K.M. (2015). SLC transporters as therapeutic targets: emerging opportunities. Nat. Rev. Drug Discov. 14, 543–560.

Ling, P.D., Tan, J., Sewatanon, J., and Peng, R. (2008). Murine Gammaherpesvirus 68 open reading frame 75c tegument protein induces the degradation of pml and is essential for production of infectious virus. J. Virol. 82, 8000–8012.

Mempel, T.R., Henrickson, S.E., and von Andrian, U.H. (2004). T-cell priming by dendritic cells in lymph nodes occurs in three distinct phases. Nature 427, 154–159.

Menon, R.P., and Hughes, R.C. (1999). Determinants in the N-terminal domains of galectin-3 for secretion by a novel pathway circumventing the endoplasmic reticulum-Golgi complex. Eur. J. Biochem. 264, 569–576.

Mercier, S., St-Pierre, C., Pelletier, I., Ouellet, M., Tremblay, M.J., and Sato, S. (2008). Galectin-1 promotes HIV-1 infectivity in macrophages through stabilization of viral adsorption. Virology 371, 121–129.

Miyagawa, I., Nakayamada, S., Nakano, K., Yamagata, K., Sakata, K., Yamaoka, K., and Tanaka, Y. (2017). Induction of regulatory T cells and its regulation with Insulin-like growth factor/insulin-like growth factor binding protein-4 by human mesenchymal stem cells. J. Immunol. *199*, 1616–1625.

Moutaftsi, M., Peters, B., Pasquetto, V., Tscharke, D.C., Sidney, J., Bui, H.-H., Grey, H., and Sette, A. (2006). A consensus epitope prediction approach identifies the breadth of murine TCD8+-cell responses to vaccinia virus. Nat. Biotechnol. *24*, 817–819.

Nangia-Makker, P., Balan, V., and Raz, A. (2008). Regulation of tumor progression by extracellular galectin-3. Cancer Microenviron. *1*, 43–51.

Nash, A.A., and Dutia, B.M. (2008). Murine gammaherpesvirus 68. In Encyclopedia of Virology, B.W.J. Mahy and M.H.V. van Regenmortel, eds. (Elsevier), pp. 372–378.

Nash, A.A., Dutia, B.M., Stewart, J.P., and Davison, A.J. (2001). Natural history of murine gamma-herpesvirus infection. Philos. Trans. R. Soc. Lond. B Biol. Sci. *356*, 569–579.

Ouellet, M., Mercier, S., Pelletier, I., Bounou, S., Roy, J., Hirabayashi, J., Sato, S., and Tremblay, M.J. (2005). Galectin-1 acts as a soluble host factor that promotes HIV-1 infectivity through stabilization of virus attachment to host cells. J. Immunol. *174*, 4120–4126.

Qian, D., and Weiss, A. (1997). T cell antigen receptor signal transduction. Curr. Opin. Cell Biol. *9*, 205–212.

Rabinovich, G.A., and Toscano, M.A. (2009). Turning "sweet" on immunity: galectin–glycan interactions in immune tolerance and inflammation. Nat. Rev. Immunol. *9*, 338–352.

Rabinovich, G.A., Baum, L.G., Tinari, N., Paganelli, R., Natoli, C., Liu, F.T., and Iacobelli, S. (2002). Galectins and their ligands: amplifiers, silencers or tuners of the inflammatory response? Trends Immunol. *23*, 313–320.

Radosavljevic, G., Volarevic, V., Jovanovic, I., Milovanovic, M., Pejnovic, N., Arsenijevic, N., Hsu, D.K., and Lukic, M.L. (2012). The roles of Galectin-3 in autoimmunity and tumor progression. Immunol. Res. *52*, 100–110.

Sano, H., Hsu, D.K., Yu, L., Apgar, J.R., Kuwabara, I., Yamanaka, T., Hirashima, M., and Liu, F.T. (2000). Human galectin-3 is a novel chemoattractant for monocytes and macrophages. J. Immunol. *165*, 2156–2164.

Sehrawat, S., Reddy, P.B.J., Rajasagi, N., Suryawanshi, A., Hirashima, M., and Rouse, B.T. (2010). Galectin-9/TIM-3 interaction regulates virus-specific primary and memory CD8+ T cell response. PLoS Pathog. *6*, e1000882.

Sehrawat, S., Kirak, O., Koenig, P.-A., Isaacson, M.K., Marques, S., Bozkurt, G., Simas, J.P., Jaenisch, R., and Ploegh, H.L. (2012). CD8(+) T cells from mice transnuclear for a TCR that recognizes a single H-2K(b)-restricted MHV68 epitope derived from gB-ORF8 help control infection. Cell Rep. *1*, 461–471.

Sehrawat, S., Kumar, D., and Rouse, B.T. (2018). Herpesviruses: harmonious pathogens but relevant cofactors in other diseases? Front. Cell. Infect. Microbiol. *8*, 177.

Slebioda, T.J., Rowley, T.F., Ferdinand, J.R., Willoughby, J.E., Buchan, S.L., Taraban, V.Y., and Al-Shamkhani, A. (2011). Triggering of TNFRSF25 promotes CD8+ T-cell responses and anti-tumor immunity. Eur. J. Immunol. *41*, 2606–2611.

Smith, L.K., Boukhaled, G.M., Condotta, S.A., Mazouz, S., Guthmiller, J.J., Vijay, R., Butler, N.S., Bruneau, J., Shoukry, N.H., Krawczyk, C.M., et al. (2018). Interleukin-10 directly inhibits CD8+ T cell function by enhancing N-glycan branching to decrease antigen sensitivity. Immunity *48*, 299–312.e5.

Toscano, M.A., Bianco, G.A., Ilarregui, J.M., Croci, D.O., Correale, J., Hernandez, J.D., Zwirner, N.W., Poirier, F., Riley, E.M., Baum, L.G., et al. (2007). Differential glycosylation of TH1, TH2 and TH-17 effector cells selectively regulates susceptibility to cell death. Nat. Immunol. *8*, 825–834.

Vasta, G.R. (2009). Roles of galectins in infection. Nat. Rev. Microbiol. *7*, 424–438.

Viola, A., Lanzavecchia, A., Sakakibara, Y., and Lanzavecchia, A. (1996). T cell activation determined by T cell receptor number and tunable thresholds. Science *273*, 104–106.

Wherry, E.J., and Ahmed, R. (2004). Memory CD8 T-cell differentiation during viral infection. J. Virol. *78*, 5535–5545.

Wherry, E.J., Ha, S.-J., Kaech, S.M., Haining, W.N., Sarkar, S., Kalia, V., Subramaniam, S., Blattman, J.N., Barber, D.L., and Ahmed, R. (2007). Molecular signature of CD8+ T cell exhaustion during chronic viral infection. Immunity *27*, 670–684.

Wong, P., and Pamer, E.G. (2003). CD8 T cell responses to infectious pathogens. Annu. Rev. Immunol. *21*, 29–70.

Yip, P.K., Carrillo-Jimenez, A., King, P., Vilalta, A., Nomura, K., Chau, C.C., Egerton, A.M.S., Liu, Z.-H., Shetty, A.J., Tremoleda, J.L., et al. (2017). Galectin-3 released in response to traumatic brain injury acts as an alarmin orchestrating brain immune response and promoting neurodegeneration. Sci. Rep. *7*, 41689.

Ziegler, A., Müller, C.A., Böckmann, R.A., and Uchanska-Ziegler, B. (2009). Low-affinity peptides and T-cell selection. Trends Immunol. *30*, 53–60.

Zinkernagel, R.M. (1996). Immunology taught by viruses. Science *271*, 173–178.

Supplemental Information

Galectin-3 Regulates γ-Herpesvirus

Specific CD8 T Cell Immunity

Manpreet Kaur, Dhaneshwar Kumar, Vincent Butty, Sudhakar Singh, Alexandre Esteban, Gerald R. Fink, Hidde L. Ploegh, and Sharvan Sehrawat

Figure S1

A

#Sample	UniqPer10M	Total	UniquelyMapping	%UniqMapping	RiboMapping	%Ribo	SpliceJunctions	%Jxns	Exon/Intron	Exon/Intergenic
Naive	0.62	98405474	74296323	75.5	475650	0.64	7411715	9.98	80.72	1859.99
Day6	0.59	107360448	82907794	77.22	986561	1.19	10282808	12.4	198.8	4125.19

#Sample	log2(m(3'/5'))	log2(m(3'/CDS))	log2(m(CDS/5'))	sd(3'/5')	sd(3'/CDS)	sd(CDS/5')	Insert size Mean (bp)	Insert size Stdv (bp)
Naive	0.38	-0.21	0.59	1.43	0.97	1.33	173.6	67.1
Day6	0.31	-0.25	0.55	1.53	1.1	1.45	179	60.3

B

Gene	Naïve RPKM	D6 RPKM	Day6/Naive
Tap1	153	147	1.041
Beta2m	2362	1743	1.3
H2(D1)	156	169	0.98

C

D

Transcripts common in OT1 and TN cells

ORF8 TN cells

Color Key

E

ORF8 TN cells   P14 tg cells

UP regulated genes   Down regulated genes
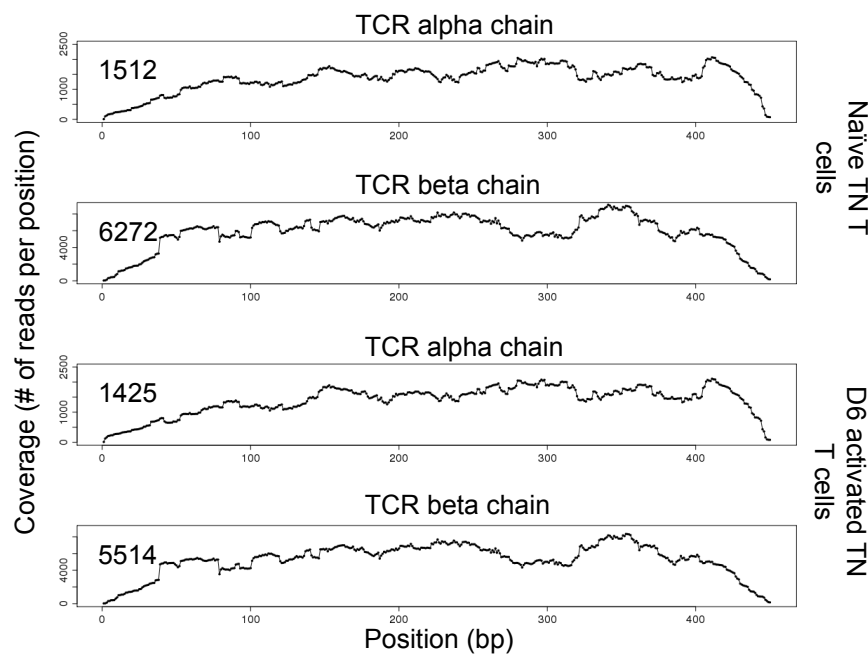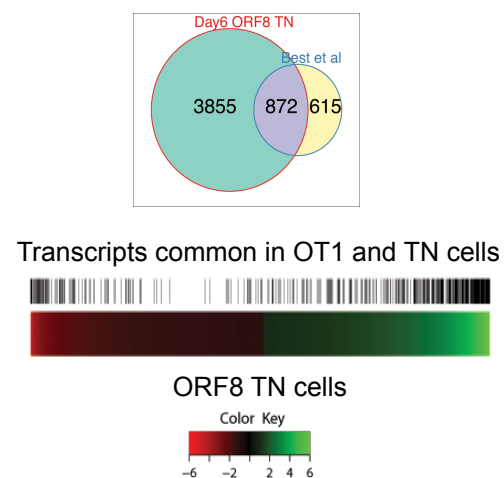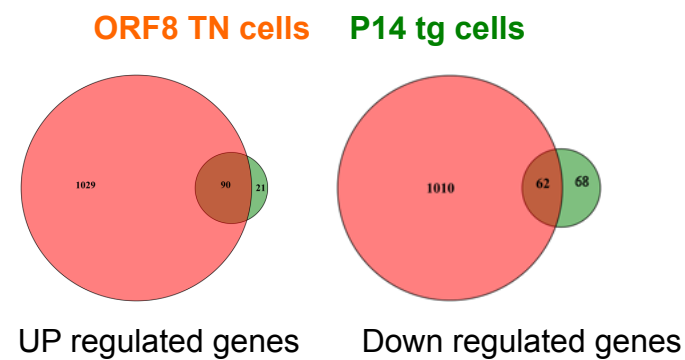
Figure S1 Analysis of RNA seq data obtained from H-2K^b-ORF8 TCR TN naïve and activated CD8$^+$ T cells to determine its quality. (Related to figure 1& 2)

A. Key attributes for analyzing the quality of RNA seq data. B. The number of reads (RPKM) recorded for some of the control genes. RPKM (Reads per kilobase per million mapped reads) = total exon reads/mapped reads (million) x exon length (Kb) C. Intensity of the reads recovered from RNAseq data present in the rearranged VDJ and VJ of β- and α-chains of TCR in naïve and activated H-2K^b-ORF8 TCR TN CD8$^+$ T cells. D-E. A comparison of transcriptome of TN cells CD8$^+$ T cells, Tg OT1 cells and Tg P14 CD8$^+$ T cells that were activated by γ-herpesvirus, Listeria monocytogenes and Lymphocytic choriomeningitis virus (LCMV) Armstrong infection respectively. D. Upper panel; Venn diagram shows the comparisons of transcriptome of OT1 cells and ORF8 TCR TN CD8$^+$ T cells that were differentially expressed atleast 1.5 fold in both the cell types. Lower panel; Heat map of 1.5 fold differentially expressed transcripts in ORF8 TCR TN CD8$^+$ T cells (lower heat map) and those that are common in OT1 cells and ORF8 TN cells (upper heat map). E. A comparison of differential transcriptome of ORF8 TN cells and P14 tg cells in the acute phase of a MHV68 and LCMV infection. Pi chart shows the numbers of genes up or down regulated by two fold in the respective cell types.

Figure S2

A

Protein class vs P- value

B

Cellular compartment vs P- value
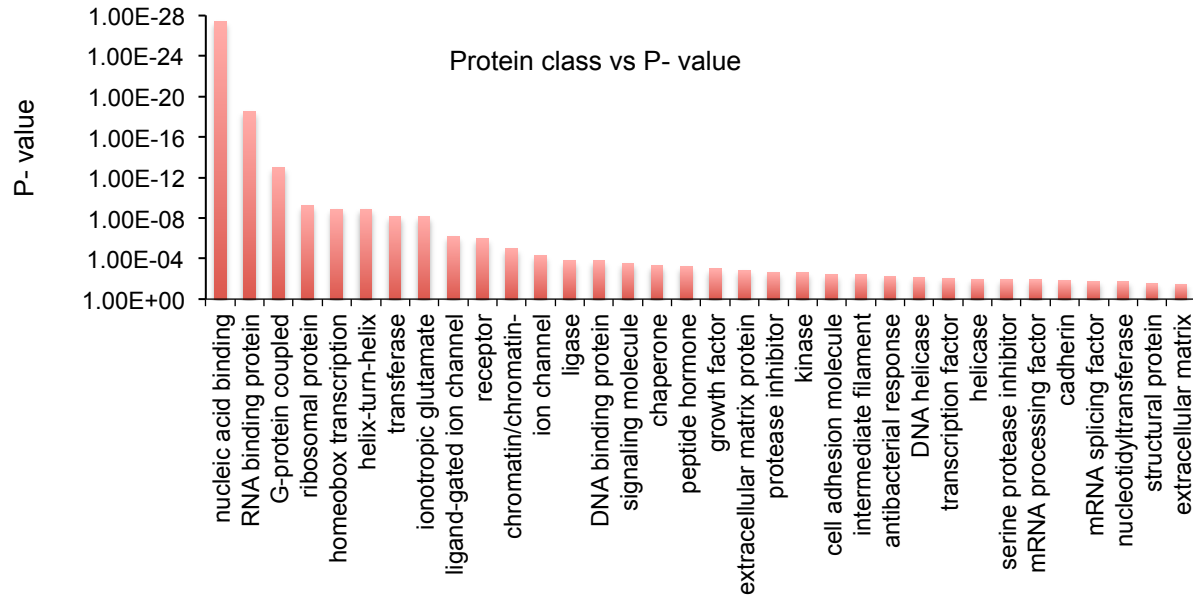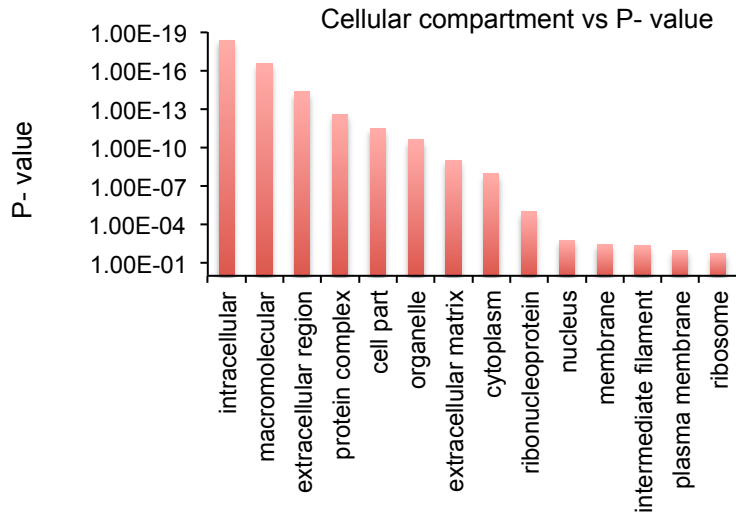
Figure S2 Gene ontology (GO) panther pathway analysis of differentially expressed transcripts in activated and naïve ORF8 TCR TN CD8$^+$ T cells. (Related to figure 1)

A. Bar diagram depicts the p-values of transcripts represented for the class of proteins. B. Bar diagram depicts the p-values of transcripts represented for cellular compartment.

Figure S3
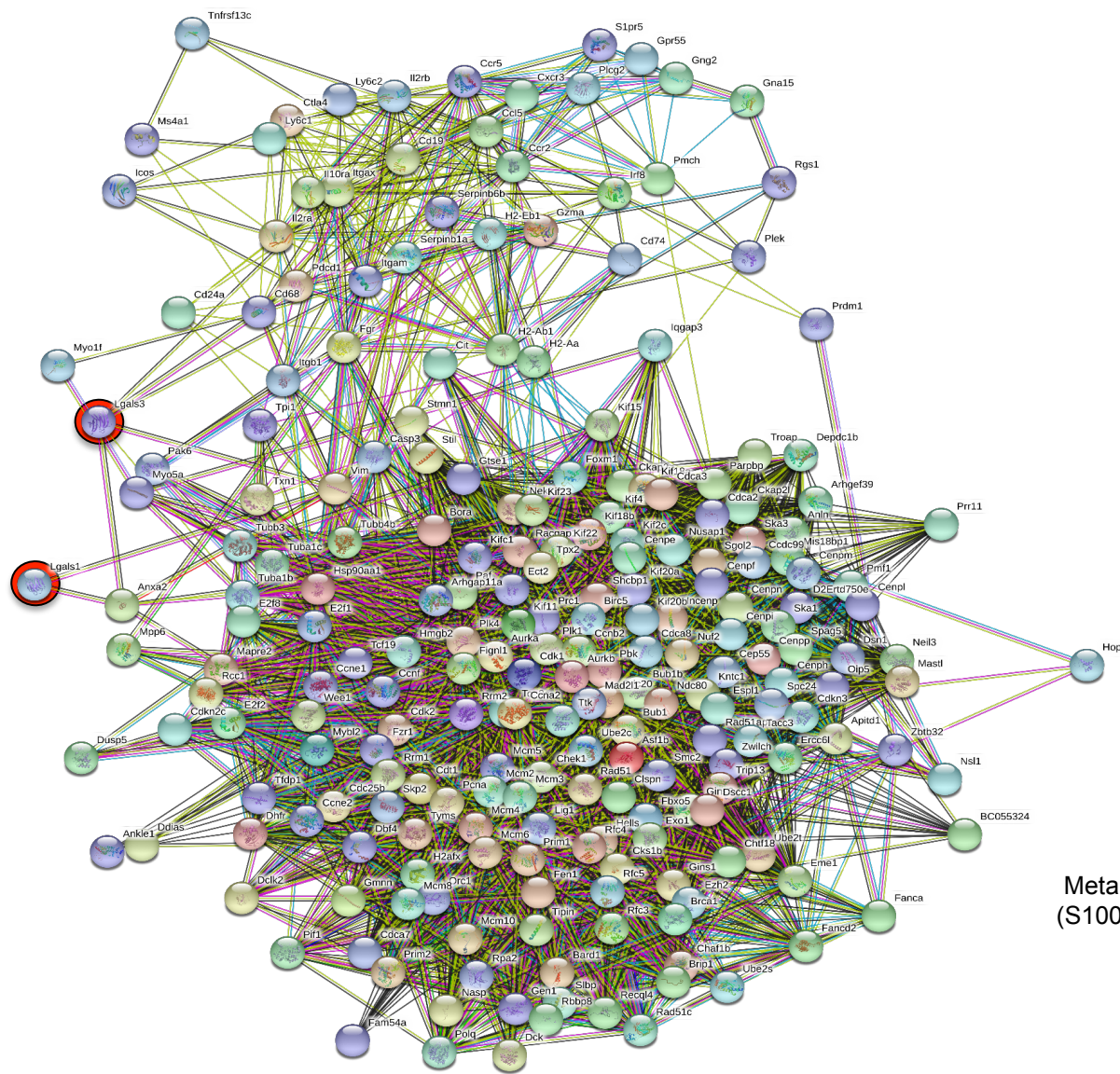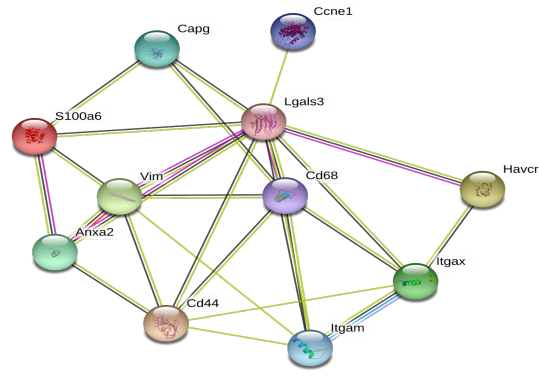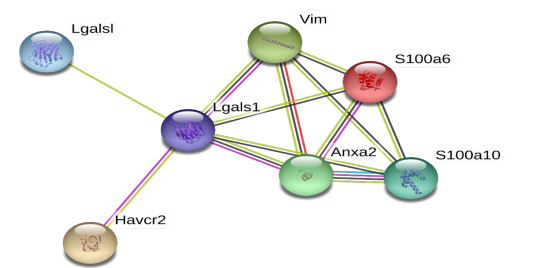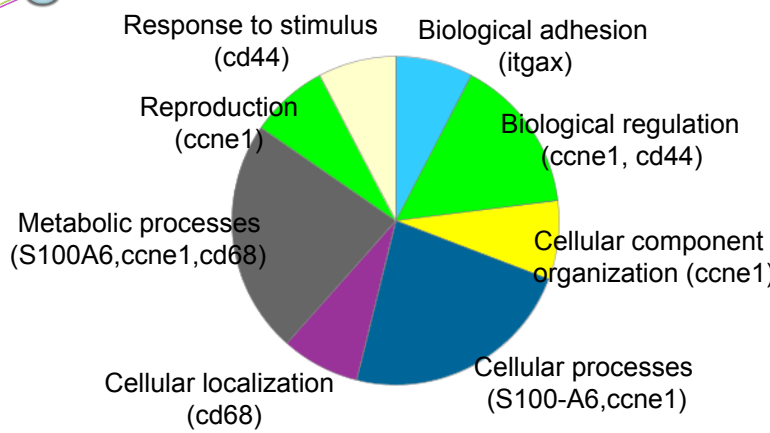
Figure S3 Computational analysis of RNAseq data to generate STRING network to investigate protein-protein interactions (PPI). (Related to figure 2)

A. STRING network of differentially expressed genes having a cut off criteria of 5RPKM in either samples and a two fold change in expression between naïve and activated TN cells. Hub genes having equal to or more than 5 interactions with a p value <1.0e-16 were used for network generation. Members of galectin family are highlighted with red circles. B and C. STRING Network is generated to show Lgals genes as hub genes, Lgals3 (B) and Lgals1(C). Lgals3 interacted with 10 partners while Lgals1 interacted with 6 partners. Both networks had a PPI enrichment p value < 1.0e-16. D. Lgals3 gene and its interacting partner (7 out of 10 genes were mapped through PANTHER) to investigate different biological process. *Itgam, capg*, and *Anxa2* were not mapped through PANTHER.

Figure S4
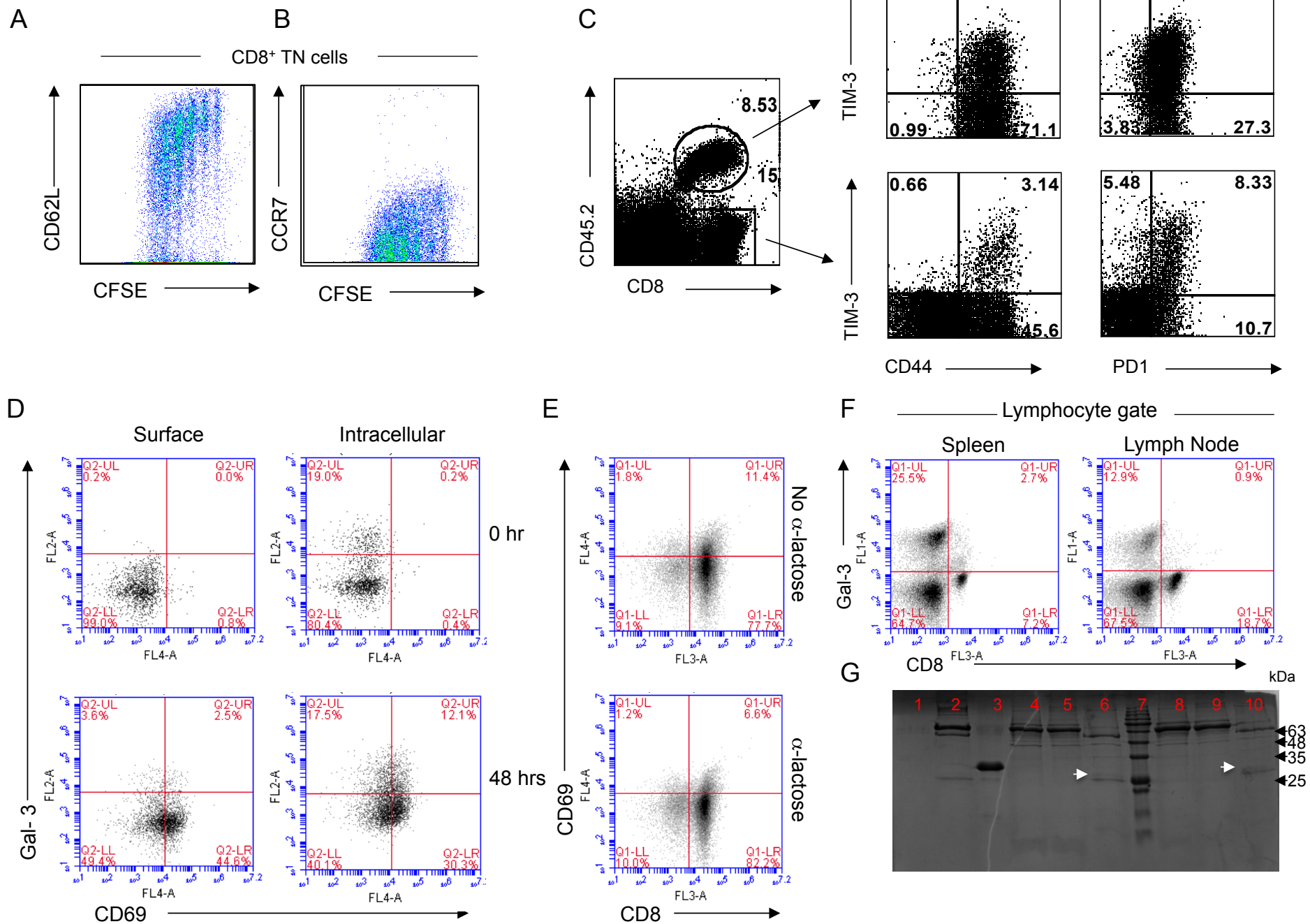
Fig S4 Analyzing the expression of some of the gene at protein level in activated TN cells as compared to naïve TN cells. (Related to figure 1 &2)

A and B. CFSE labeled ORF8 TN T cells were stimulated with BMDCs pulsed with the cognate KNYIFEEKL peptide for three days. Representative FACS plots show the expression of CD62L (A) and CCR7 (B) in dividing TCR TN CD8$^+$ T cells. Representative FACS plots are shown. C. Representative FACS plots show the expression of TIM-3 and PD1 by donor and endogenous CD8$^+$ T cells. For each experiment at least four animals were included and experiments were repeated two times with similar results. D. *In vitro* activation of magnetically sorted CD8$^+$ T cells using anti-CD3 (coated) and CD28 (soluble) antibodies to measure intracellular (permeabilized cells) and surface (without permeabilization) galectin-3. The cells were stimulated for two days and the expression level of galectin-3 were measured as described in transparent methods section. Activated cells predominantly up regulated intracellular galectin-3 but its expression on cell surface was affected to a lesser extent. E. Measuring the influence of a-lactose on CD8$^+$ T cell activation. CD8$^+$ T cells were purified from lymph node of C57BL/6 mouse and incubated with 277mM of α-lactose for 1 hour at 37°C. The cells were then washed three times with PBS and stimulated with anti-CD3 (coated) and anti-CD28 (soluble) for 12 hrs at 37°C. After activation the cells were washed and stained with anti-CD69 and anti-CD8 antibodies. F-G. A demonstration that the clone (B2C10) of antibody used for neutralization of galectin-3 can bind and detect extracellular surface expressed galectin-3. F. Splenocytes from C57BL/6 mice were isolated to stain for CD8 and galectin-3. Gated lymphocytes are shown for anti-CD8 and galectin-3 stainings. While CD8$^+$ T cells expressed low levels of galectin-3, CD8$^-$ T cells demonstrate significant population of surface galectin-3 expressing cells. G. A galectin-3 pull-down by the neutralizing antibody (B2C10) from the lysates of spleen cells and lymph node cells. Different samples prepared from pull down experiments were resolved on a 12% SDS-PAGE. lane 1: dye, lane 2: beads with IgG1 (blocking antibody, 3μg), lane 3: recombinant galectin 3 (3μg), lane 4: input splenocytes lysate, lane 5: residual sample from splenocytes lysate after pull-down, lane 6; pull-down fraction from splenocytes lysate, lane 7: molecular weight marker (MWM), lane 8: input lymph node cell lysate, lane 9: residual sample from splenocytes lysate after pull-down, lane 10: pull-down fraction from lymph node cells. In lanes 6 and 10, a faint band of galectin-3 corresponding to 30kDa is retrieved (white arrow marked), bonds corresponding to heavy chain (~50kDa) and light chain (25kDa) of IgG1 molecules are also visible. High molecular mass bands might represent aggregated products and the carrier protein in antibody preparation.

Figure S5
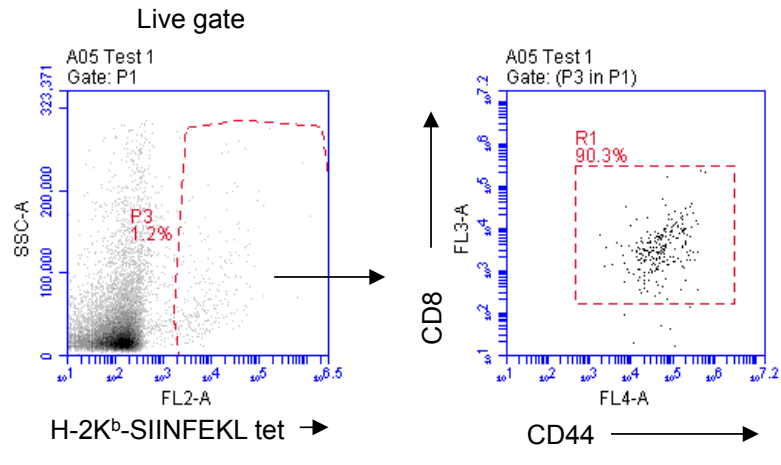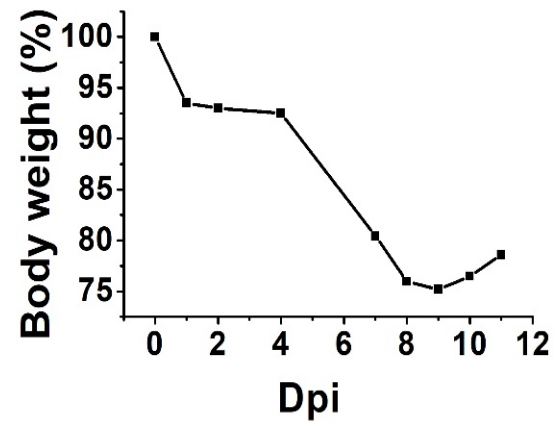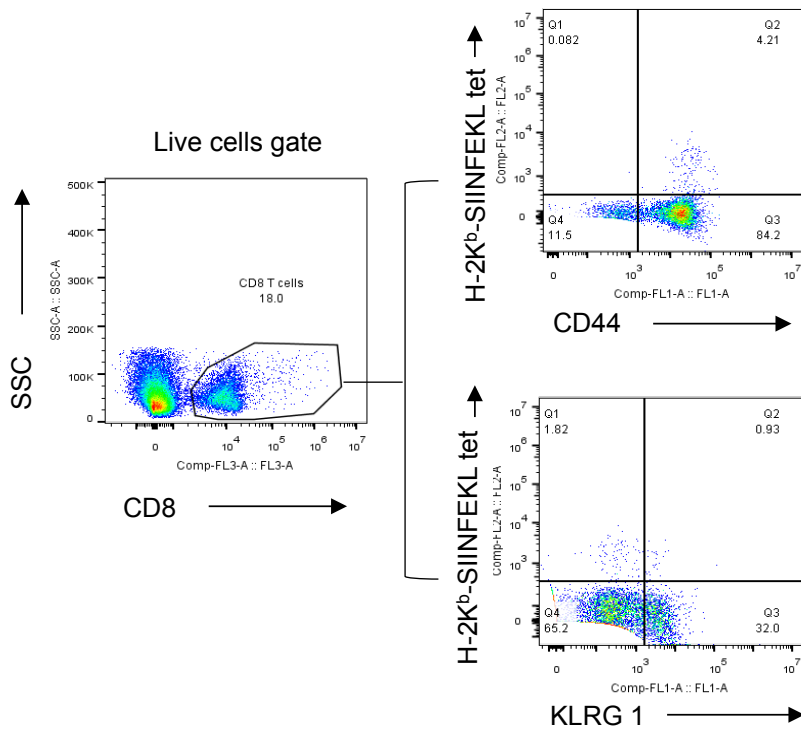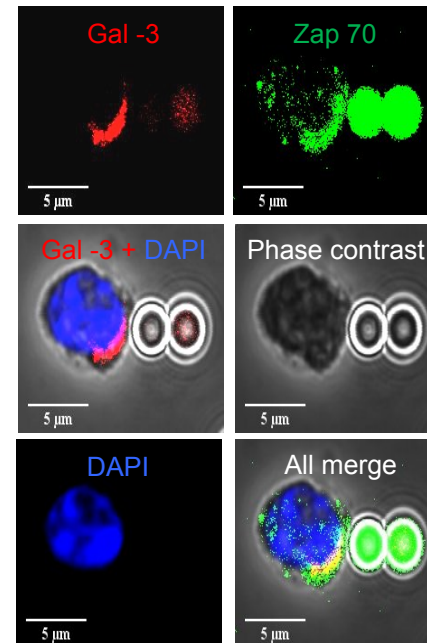
Figure S5 Phenotypic analysis of antigen-specific CD8+ T cells obtained from mice infected with MHV68 M2-SIINFEKL and WSN-SIINFEKL. (Related to figure 5)

A. 50x10^3 OT1 cells were transferred into C57BL/6 mice, which were then infected with MHV68 M2-SIINFEKL through intranasal route. On 5dpi, PBMCs were analyzed for SIINFEKL specific CD8+ T cells. Representative FACS plots are shown. B-D. C57BL/6 mice were infected with WSN-SIINFEKL through intranasal route and disease progression and phenotypic analysis of antigen-specific CD8+ T cells was measured. B. Body weight of infected animals was monitored for up to 12 days and is shown as change in body weight as compared to the original. C. On 6dpi, mediastinal LN single cell suspensions were analyzed for the phenotype of endogenous SIINFEKL specific CD8+ T cells. Representative FACS plots are shown. D. H-2K^b-SIINFEKL-specific CD8+ T cells were magnetically sorted and analyzed for co-localization of galectin-3 and Zap70 towards the immune synapse. Representative confocal images are shown.

Figure S6

A

Gal-3   Zap70   Merge

B

a-CD8 T cells

C

Gal-3 at IS

D
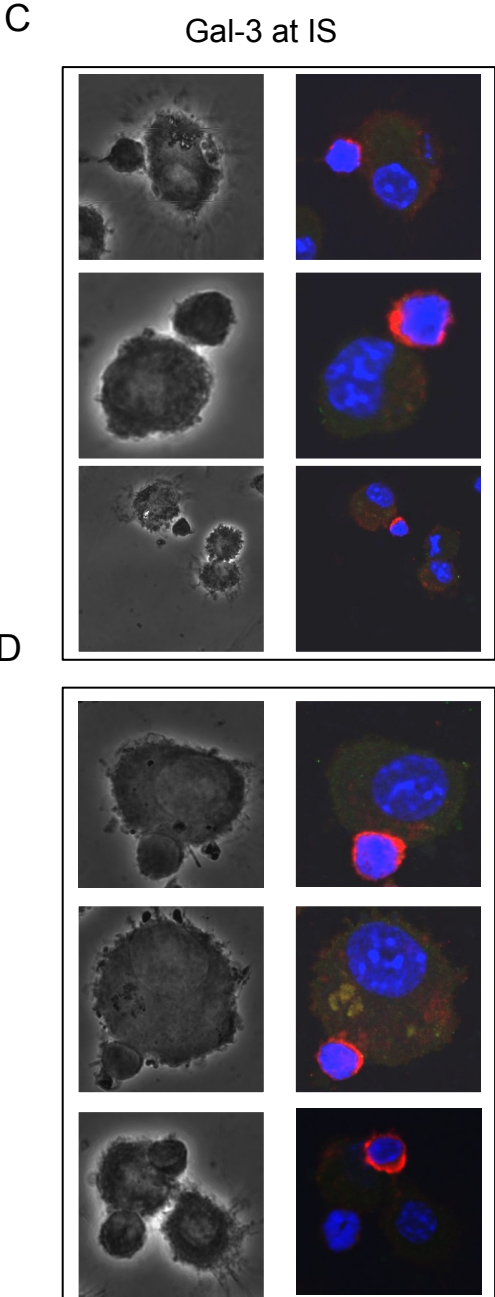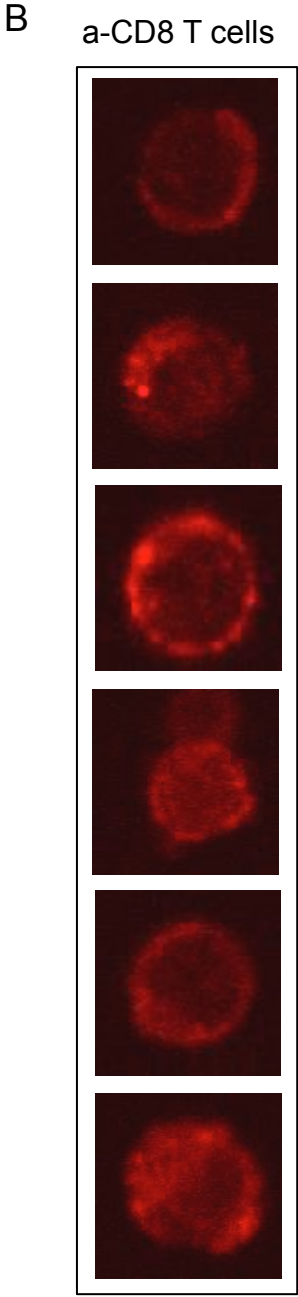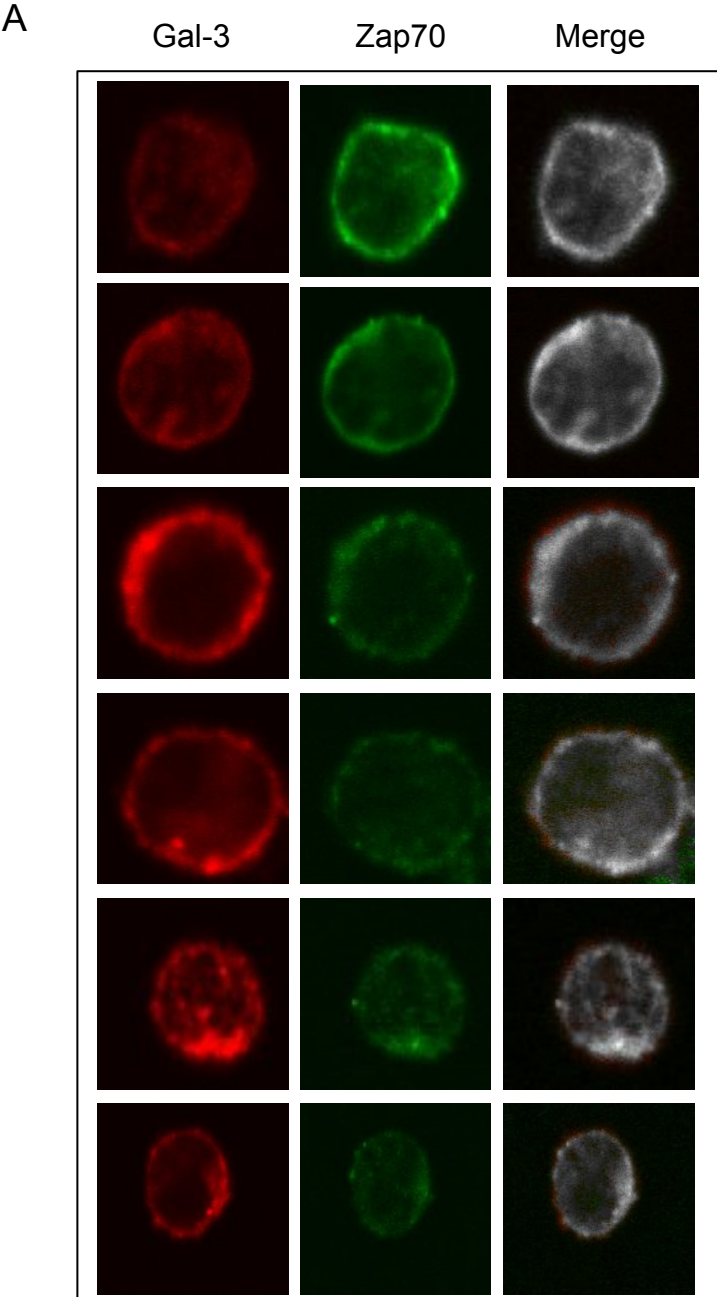
Figure S6 Additional images to demonstrate the recruitment of galectin-3 at immunological synapse. (Related to figure 4)

A. Previously activated OT1 CD8$^+$ T cells during infection of naïve OT1 recipient mice with MHV68-M2-SIINFEKL were isolated during the acute phase of response at 6dpi and analyzed for co-localization of galectin-3 and Zap70. Six representative images are shown. B. Representative images of sorted OT1 cells incubated in the absence of peptide pulsed APCs. C-D. Representative images to demonstrate recruitment of OT1 cells' expressed galectin-3 at immunological synapse upon incubation with SIINFEKL pulsed APCs at 10min (C) and 1hr (D).

Figure S7

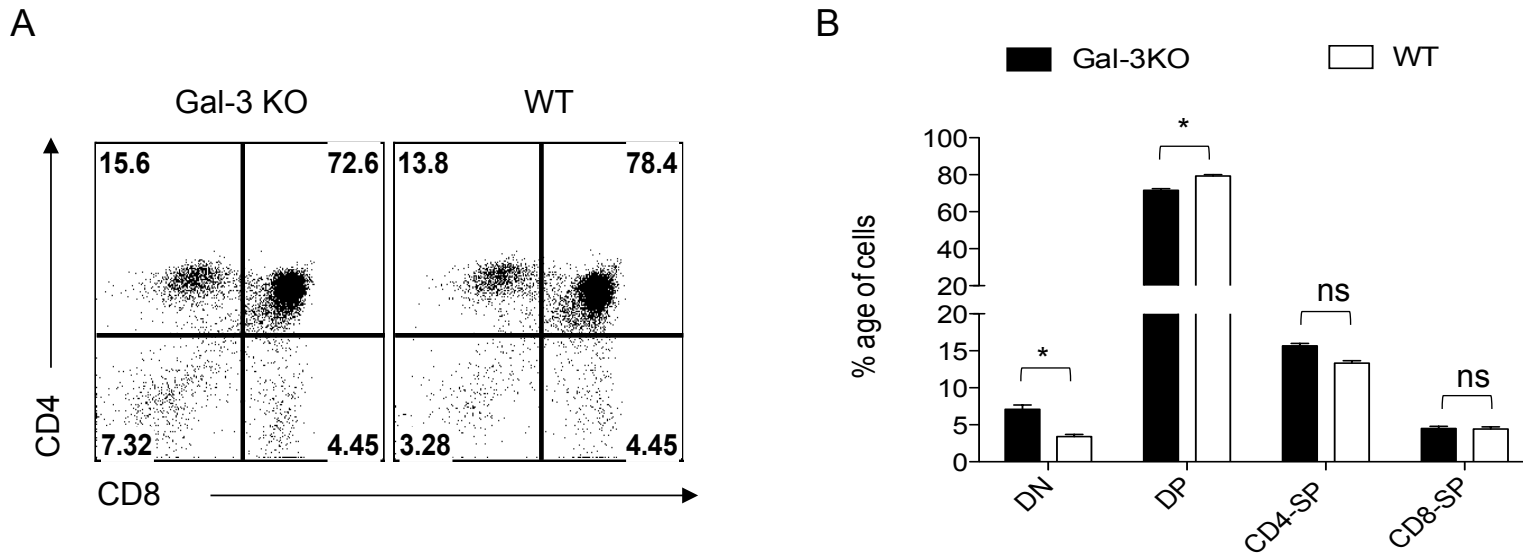
Figure S7 Comparison of thymic cellular distribution in galectin-3 KO and WT animals. (Related to figure 6 to 9)

A. FACS plots show the frequencies of single positive, double positive and double negative for CD4$^+$ and CD8$^+$ T cells. B. Bar diagram represent the frequencies of indicated cell populations from four animals in each group.

0610007P14Rik	1810043G02Rik	4632434I11Rik	AI467606	BC094916	D14Abb1e	Gm9846	Mll5	Phf17	Wdr20a	Zfp526
0610009D07Rik	2010012O05Rik	4833420G17Rik	AI597468	Beta-s	D4Wsu53e	Gpi1	Mnf1	Pion	Wdr67	Zfp579
0610010F05Rik	2010015L04Rik	4930422G04Rik	AI837181	Bloc1s2a	D5Ertd579e	Grlf1	Mrp63	Rab1	Wdr85	Zfp580
0610010K14Rik	2010107E04Rik	4930427A07Rik	AI846148	Bmyc	D8Ertd82e	Gtpbp5	Nrp	Rnaset2a	Zfp110	Zfp592
0610030E20Rik	2010111I01Rik	4930432K21Rik	AK010878	C030006K11Rik	Ddx39	Gyg	Nt5c3l	Rnaset2b	Zfp12	Zfp652
0610037L13Rik	2210016L21Rik	4930444A02Rik	Akr1b3	C030046E11Rik	Dnahc8	Gyk	Nup62-il4i1	Rpl34-ps1	Zfp146	Zfp653
1110004F10Rik	2210404J11Rik	4930453N24Rik	Akr1e1	C230052I12Rik	Dnalc4	H2-Ke2	Pagr1a	Rpl36al	Zfp182	Zfp661
1110008F13Rik	2210404O07Rik	4930486L24Rik	Anks1	C330006A16Rik	Dnase2a	H2-Ke6	Pcdhga1	Rps3a1	Zfp207	Zfp664
1110008J03Rik	2300009A05Rik	4930503L19Rik	Atad3a	C330027C09Rik	E130309D02Rik	H2-T9	Pcdhga10	Serpinb6a	Zfp260	Zfp672
1110008P14Rik	2310011J03Rik	4930579G24Rik	Atp5k	C87436	E130311K13Rik	H3f3b	Pcdhga11	Sfrs18	Zfp276	Zfp687
1110034G24Rik	2310022B05Rik	4932438A13Rik	Atpbd4	C920025E04Rik	E330009J07Rik	Hba-a1	Pcdhga12	Solh	Zfp280c	Zfp692
1110059E24Rik	2310035C23Rik	4933434E20Rik	AU022252	Calm2	E430025E21Rik	Hba-a2	Pcdhga2	Spata5l1	Zfp280d	Zfp71-rs1
1190002N15Rik	2310039H08Rik	5730508B09Rik	AW549877	Calm3	Eef1b2	Hist1h4c	Pcdhga3	Spin2	Zfp281	Zfp710
1190007I07Rik	2310042D19Rik	5830415F09Rik	AW554918	Car12	Efha2	Hist1h4i	Pcdhga5	Stx4a	Zfp287	Zfp74
1300018J18Rik	2410066E13Rik	6030458C11Rik	B630005N14Rik	Car15	Eif2c1	Hmga1-rs1	Pcdhga6	Stxbp3a	Zfp318	Zfp740
1500009L16Rik	2410131K14Rik	6330403M23Rik	B930041F14Rik	Car2	Eif2c2	Hnrpll	Pcdhga7	Supt16	Zfp329	Zfp770
1500032L24Rik	2510002D24Rik	6330416G13Rik	Baat1	Car5b	Eif2c3	Hras1	Pcdhga8	Supt20	Zfp335	Zfp771
1600002H07Rik	2610019F03Rik	8430410A17Rik	BC003965	Ccdc90a	Fam108c	Jhdm1d	Pcdhga9	Supt4a	Zfp354c	Zfp784
1600014C10Rik	2610301B20Rik	9030617O03Rik	BC004004	Cd24a	Fam86	Klhdc5	Pcdhgb1	Sypl	Zfp365	Zfp821
1700017B05Rik	2700029M09Rik	9430023L20Rik	BC016423	Cenpc1	Fam92a	Klra12	Pcdhgb2	Tgtp2	Zfp367	Zfp827
1700020L24Rik	2700060E02Rik	9930012K11Rik	BC029214	Chmp1b	Fasl	Klra23	Pcdhgb4	Tmem170	Zfp369	Zfp85-rs1
1700025G04Rik	2700094K13Rik	9930104L06Rik	BC030336	Cldn25	Fem1a	Lrdd	Pcdhgb5	Tmem48	Zfp382	Zfp865
1700037H04Rik	2810403A07Rik	A130010J15Rik	BC030867	Cnih	Fh1	Lrrc33	Pcdhgb7	Tmem8	Zfp422	Zfp932
1700066M21Rik	2810417H13Rik	A230046K03Rik	BC037034	Csda	Gbp3	Lsmd1	Pcdhgb8	Tmsb15b2	Zfp445	Zkscan14
1700088E04Rik	3010026O09Rik	A230050P20Rik	BC048403	Ctps	Gm13826	Man1a	Pcdhgc3	Trp53	Zfp451	Zkscan6
1700094D03Rik	3110057O12Rik	A430005L14Rik	BC049715	Cxx1b	Gm20604	Mettl21d	Pcdhgc4	Trp53bp2	Zfp507	Znrd1as
1810013L24Rik	3230401D17Rik	A730008H23Rik	BC052040	Cyp4v3	Gm5506	Mll1	Pcdhgc5	Trp53i13	Zfp513	
1810022K09Rik	4632415K11Rik	AA414768	BC055324	Cyp51	Gm5918	Mll2	Pgm1	Txn1	Zfp518a	
1810037I17Rik	4632428N05Rik	AB124611	BC056474	D030056L22Rik	Gm6251	Mll3	Phf15	Ube2cbp	Zfp523	

Table S5 -Hub genes and their numbers of interactions (Cut Off ≥5 interactions) (Related to figure 2 & 3)

Genes	Interaction	Genes	Interaction	Genes	Interaction	Genes	Interaction
Mcm5	141	Cdkn3	55	Rfc4	27	Cdc25b	11
Prc1	136	Ckap2	55	Kif15	26	Fanca	11
Mad2l1	129	Ccne1	54	Tyms	26	Zbtb32	11
Kif20a	125	Fzr1	54	Racgap1	26	Ube2s	11
Rad51ap1	119	Ercc6l	54	Rad51c	26	Tpi1	11
Top2a	118	Fignl1	54	Tuba1b	25	Pak6	11
Smc2	117	Kif22	53	Nasp	24	Bard1	10
Zwilch	116	Kntc1	52	Dscc1	24	Plcg2	10
Cenpf	114	Rpa2	52	Fancd2	23	Cd24a	10
Kifc1	111	Rfc3	51	Tubb3	23	**Lgals3**	**10**
Cdca8	109	Gins2	51	Myo5a	22	Il10ra	10
Ect2	107	Kif23	51	Pbk	21	Hsp90aa1	9
Lig1	105	Tipin	51	Tuba1c	21	Cit	9
Cep55	103	Ccne1	51	Wee1	20	Ly6c2	9
Birc5	102	Anln	50	E2f2	20	Il2ra	9
Kif20b	101	Ccna2	50	Tubb4b	20	Cdkn2c	9
D2Ertd750e	101	Bub1	50	Pmf1	20	H2-Aa	8
Ube2c	100	Ezh2	50	H2-Ab1	20	Fbxo5	8
Ttk	98	Gen1	49	Cdca3	20	Kif11	8
Cdca2	97	H2afx	48	Polq	20	S1pr5	8
Rfc5	92	Rrm1	48	Shcbp1	20	Tnfrsf13c	8
Tacc3	92	Cenpn	47	Cd68	20	Vim	8
Oip5	90	Arhgef39	46	Mcm4	19	Dck	8
Mcm3	89	Mcm8	46	Stil	18	Ly6c1	8
Kif2c	89	Ccne2	45	E2f8	18	Irf8	8
Mcm2	88	Pcna	45	Prr11	18	Gng2	7
Spc24	88	Rad51	45	Mcm10	17	Anxa2	7
Cenpi	88	Cdca7	45	Il2rb	17	Prdm1	7
Arhgap11a	88	Parpbp	44	Itgb1	17	Plek	7
Espl1	86	Tpx2	43	Ska3	17	Mapre2	7
Cenph	86	Depdc1b	42	Trip13	16	Ankle1	7
Ccnf	83	Cks1b	40	Fam54a	16	Nsl1	6
Nusap1	81	E2f1	39	Cdk1	15	Gna15	6
Cenpe	79	Gins1	39	Rbbp8	15	**Lgals1**	**6**
Kif4	75	Neil3	38	Apitd1	15	Dhfr	6
Ccdc99	75	Slbp	37	Bora	15	Mpp6	6
Bub1b	74	Tfdp1	35	Pif1	15	Cd74	5
Orc1	74	Cenpl	34	Itgax	15	Gmnn	5
Clspn	74	Nuf2	34	Serpinb1a	15	Cdt1	5
Dbf4	73	Eme1	34	Serpinb6b	15	H2-Eb1	5
Hmgb2	69	Itgam	34	Mastl	15	Cdc20	5
Exo1	67	Troap	33	Aurkb	14	Asf1b	5
Cenpm	67	Casp3	33	Ccr2	14	Txn1	5
Tcf19	67	Plk4	32	Cxcr3	14	Pmch	5
Plk1	64	Mcm6	32	Chaf1b	14	Gpr55	5
Ccnb2	64	Prim1	31	Kif18b	14	Gzma	5
Skp2	64	Recql4	31	Ccl5	14	Mybl2	5
Chek1	62	Fen1	31	Prim2	13	Brca1	5
Foxm1	61	Hells	30	Rrm2	13	Pdcd1	5
Spag5	61	Ndc80	29	Cenpp	13	Ctla4	5
Ska1	60	Ccr5	29	Dclk2	13	Icos	5
Gtse1	60	Kif18a	28	BC055324	13	Rgs1	5
Ckap2l	60	Incenp	28	Iqgap3	13	Hopx	5
Chtf18	59	Cdk2	28	Cd19	12	Dusp5	5
Paf	57	Sgol2	28	Ms4a1	12	Myo1f	5
Mis18bp1	56	Brip1	28	Stmn1	12	Ddias	5
Aurka	55	Ube2t	27	Rcc1	12		
Dsn1	55	Nek2	27	Fgr	12		

Transparent Methods

Mice, virus and cell lines used

Murine γ-herpesvirus (MHV68)-specific CD8$^+$ T cell transnuclear (TN) mice were generated and bred onto a C57BL/6 Rag1$^{-/-}$ background (Sehrawat et al., 2012). TCR TN mice, C57BL/6 mice WT mice, OT1 TCR transgenic (tg) mice and galectin-3 knock out (KO) mice were bred and maintained at the AALAC-accredited animal facility of the Whitehead Institute for Biomedical Research, Cambridge, MA or at the Small Animal Facility for Experimentation at the Indian Institute of Science Education and Research Mohali. Age and gender-matched mice were used for experiments. All studies were carried out in accordance with procedures approved by the Massachusetts Institute of Technology Committee on Animal Care (CAC protocol # 1011-123-14) and Institute Animals Care and Use Committee (IACUC) of IISER Mohali. Whitehead Institute's Animal Welfare Assurance was approved and the approval number is 11/3/2009 (IACUC, A3125-01). Institutional Animal Ethics Committee (IAEC) of Indian Institute of Science Education and Research Mohali (IISER Mohali), constituted by the Committee for the Purpose of Control and Supervision of Experiments on Animals (CPCSEA) which is established under Chapter 4, Section 15(1) of the Prevention of Cruelty to Animals Act 1960. IAEC approved all the protocols and their numbers are; (IISERM/SAFE/PRT/2016/008, 009 and IISERM/SAFE/PRT/2017/011). All the experiments were performed strictly in accordance with the approved protocols. The cell lines (Vero cells, 3T12-3 and MDCK were obtained from ATCC. All the viruses used were described earlier (Sehrawat et al., 2013). The MHV-68, its recombinant version encoding for a SIINFEKL peptide (MHV68-M2 SIINFEKL) and influenza virus encoding SIINFEKL (WSN-SIINFEKL) were grown in 3T12-3 and MDCK cells respectively and stored at −80°C until further use.

Antibodies and Other Reagents

Fluorochrome-conjugated antibodies against mouse CD16/32, CD3ε, CD8a, CD4, CD62L, CD69, CD44, B220, IFN-γ, CD11c, CD11b, CD45.1, CD45.2, PD1, KLRG1, TIM-3 and CCR7 were purchased from BD PharMingen. Anti-galectin-3 alexafluor 647 and anti-galectin-3 PE antibody were obtained from eBioscience. Anti-Zap70-FITC was obtained from BD biolegend. A neutralizing anti-galectin-3 antibody (clone B2C10) was obtained from Thermofisher Scientific. Peptides were either synthesized in house at the Massachusetts Institute of Technology biopolymer facility or were obtained from GL Biochem. H-2K^b tetramers loaded with the indicated peptides were generated and used essentially as described (Altman et al., 1996). Tetramers carrying different peptides were generated by photochemical exchange of a conditional ligand (Bakker et al., 2008). The peptide used for tetramer generation and intracellular cytokine staining (ICCS) assays include those derived from ORF9 (SVYGFTGV; H-2K^b restricted) and ORF75c (KSLTYYKL; H-2K^b restricted, SAIENYETF; H-2D^b restricted) for early antigens and ORF6 (AGYIYYQL; H-2K^b restricted, AGPHNDMEI; H-2D^b restricted), ORF8 (KNYIFEEKL; H-2K^b restricted), ORF17 (SAITNHAAF; H-2D^b restricted) and ORF61 (p79) (TSINFVKI; H-2K^b restricted). For some experiments chicken ovalbumin-derived SIINFEKL peptide was used to probe OT1 or the endogenous cells.

Isolation of CD8$^+$ T cells

In order to isolate minimally manipulated CD8$^+$ T cells, negative selection kits from Miltenyi Biotec, Stem cell technology or Dynabeads™ Mouse CD8$^+$ T cells isolation kits were used. The purity of the CD8$^+$ T cells thus obtained was ascertained by flow cytometry. All procedures for cell separation were performed as per manufacturer's instructions. For some experiments cell sorting of fluorescent antibody-labeled cells was performed using a FACSaria II or FACSfusion instruments. The desired cell populations were obtained via a "dump" gate using antibodies against markers specific for cells other than CD8$^+$ T cells. For some experiments, antigen-specific

CD8^{+} T cells were isolated from infected mice using magnetic beads coated with class I MHC monomers.

Adoptive transfer of cells and virus infection

50×10^3 negatively separated MHV68-gB-ORF8-TCR TN cells from H-2K[b] -MHV68-gB-ORF8-TCR TN mice were adoptively transferred intravenously into CD45.1 congenic C57BL/6 or WT C57BL/6 mice one day before intra peritoneal infection with 5×10^5 pfu of MHV68. In some experiments OT1 cells obtained from OT1 TCR tg mice were transferred in WT C57BL/6 mice, which were then infected with 5×10^5 pfu of MHV68 M2-SIINFEKL. In order to measure responses of endogenous memory CD8^{+} T cells, an intranasal infection of 10 weeks old mice with WSN-SIINFEKL (5×10^2 pfu) was performed. The body weight was measured until 12 days post infection (dpi). Infected animals were euthanized using CO_2 asphyxiation at different dpi for further analyses. Single cell suspensions obtained from lymphoid organs were analyzed for the number and phenotype of expanded cells. WT and Gal-3 KO mice were infected with MHV68 by intraperitoneal or intranasal route. Lymphoid organs were analyzed to measure CD8^{+} T cell responses. Lung tissues were collected to estimate viral loads.

RNA sequence analysis

FACS-purified naïve and MHV68 expanded K[b]-ORF8-TCR TN Rag1^{-/-} CD8^{+} T cells were used for RNA isolation. The purity of sorted cells was verified by flow cytometry and was routinely > 99 percent. RNA was isolated from sorted cells using a kit from Qiagen. A Trueseq RNA sample Prep kit v2 from Illumina was used for RNA processing. 1µg of input total RNA was used and 18 cycles of PCR were performed and libraries were constructed. Paired end sequencing was performed. The sequence was mapped to mm9 using ELAND tool. Reads were counted in exons REFSEQ transcripts. Then, the count was normalized for reads per kb of mRNA per million (RPKM). For most analyses, transcripts below 5RPKM in paired samples

were eliminated and genes that were selected had a more than 1.5 fold or more than two-fold difference in any comparison as indicated in figure legends.

Network analysis for SDE genes in ORF8 TCR-TN mice infected with MHV-68

Using a cut off of 5 RPKM for any genes in either of the conditions and two fold differential expression, we selected 1667 significantly differentially expressed (SDE) genes for network analysis. Network analysis was done using STRING (Search Tool for the Retrieval of Interacting Genes, https://string-db.org/) online tool. To filter out noise from the signals, we used stringent conditions. We obtained a protein-protein interaction (PPI) network that had an enrichment p value of less than 1.0e-16. Network with 498 SDE genes forming Nodes out of 1667 was obtained with STRING using default parameters. The STRING generated a .tsv file as an output that contained node1 (gene of our interest), node 2 (interacting partner). The .tsv file (output from STRING) were opened in excel and analyzed for hub genes. Genes having more than five interacting partners yielded a total of 229 hub genes (Table S5). A gene was considered as a hub gene if it had more than 5 degree of centrality. The degree of centrality $Cd(i) = deg(i) = |N(i)|$, where deg (i) is the degree of node (i), and |N(i)| is the number of neighboring nodes to the node (i) (Pavlopoulos et al., 2011). To further resolve the initially generated STRING network (that had genes which were not interacting), hub gene network was further made by STRING. Finally STRING network was generated to show Lgals genes as hub genes.

Phenotypic analysis of cells using flow cytometry

Spleen samples were extracted from different groups of animals and single cell suspensions were prepared. 1×10^6 splenocytes were used for surface staining. Prior to the addition of specific antibody, cells were blocked with anti-Fc receptor antibody (CD16/32) for 20 min at 4°C. 1µg/ml of respective fluorochrome-labeled antibodies was added to the cell suspension and incubated for 30 minutes. After three rounds of washing with PBS-2%FCS, cells were analyzed by flow cytometry. To measure the

relative expression of galectin-3 intracellularly and on the surface of activated cells, we performed surface staining as well as intracellular staining. Splenocytes from C57BL/6 mice were activated with anti-CD3 and anti-CD28 for 48 hrs at 37 degree C. After different time intervals cells were stained with anti-galectin 3, anti- CD69 and anti-CD8. For intracellular cytokine staining (ICCS), 1×10^6 of freshly isolated splenocytes or LN cells were cultured in 96-well round-bottomed plates in the presence of various concentrations of the indicated peptides and brefeldin A (5µg/ml) for 5 hr at 37°C in a humidified CO_2 incubator. At the end of the incubation period, cell surface staining, followed by ICCS was performed using a cytofix/cytoperm kit (BD Bioscience) as per manufacturer's instructions. Stained cells were analyzed flow cytometry using a FACScalibur (BD Bioscience) instrument and data were analyzed using Flowjo software (Tree star, OR). Cells were then analyzed by flow cytometry.

Immunofluorescence staining, confocal microscopy and co-localization analysis

To examine co-localization of galectin-3 with other molecules involved in immunological synapse formation during antigen-specific CD8^{+} T cell activation, we performed confocal microscopy. SIINFEKL-specific endogenous or OT1 cells were activated by any of the following three approaches; class I MHC tetramer (H-2K[b] - SIINFEKL-tetramers-allophycocyanin)-coated coverslips, SIINFEKL-peptide pulsed BMDCs or magnetic beads coated with H-2K[b]-SIINFEKL monomers. We investigated co-localization of galectin-3 with TCR marked by SIINFEKL peptide-loaded class I MHC tetramer (H-2K[b] -SIINFEKL-tetramer-allophycocyanin) and Zap70, a TCR-CD3 ζ-chain associated protein kinase involved in the initial stages of TCR signaling Confocal laser scanning microscope from Olympus (FV10i-LIV / FV10i-DOC) that has a speed of 1.1 fps having 256 x 256 - 1024 × 1024 pixel resolution and FV10i-DOC: NA 0.4 /NA 1.35 objective was used for acquiring images. Fiji software was used for analyzing the images. This software was used to calculate the Pearson's correlation coefficient (PCC) for co-localization of the probes used as described

5

elsewhere (Dunn et al., 2011). To ascertain whether or not galectin-3 produced by CD8^{+} T cells act intracellularly or extracellularly to control their activation, we performed neutralization experiments using α-lactose. α-lactose compete with galectins for their binding to carbohydrates and blocks the interaction (Demetriou et al., 2001). SIINFEKL peptide pulsed BMDCs were co-cultured with OT 1 cells in the presence of absence of 100 mM of α-lactose solution and the extent of localization of galectin-3 towards immune synapse was measured. Atleast 35 cells were counted for each group for calculating co-localization percentages for different molecules. Different methods of activation of CD8^{+} T cells for confocal imaging are described in subsequent sections. To measure whether or not α-lactose indeed works we measured the response of CD8^{+} T cells in separate experiments. CD8^{+} T cells were purified from lymph nodes of C57BL/6 mice and incubated with similar dose of α-lactose for 1 hour at 37 C. The cells were then was then washed three times with PBS and stimulated with anti-CD3 (coated) and anti-CD28 (soluble) for 12 hrs at 37 degree C. After activation, the cells were washed and stained with anti-CD69 and CD8 antibodies.

Activation of CD8^{+} T cells with MHC I tetramers

Class I MHC (H-2K[b]) SIINFEKL tetramer (allophycocyanin dye-conjugated) was coated on poly-lysine (Sigma Aldrich)-treated coverslips overnight at 4°C. The next day, coverslips were washed with sterile PBS and complete RPMI. SIINFEKL specific Sorted CD8 T cells were added to these coverslips and incubated for different time intervals. Control cells were immobilized on poly-lysine treated coverslips in the absence of Class I MHC (H-2K[b]) SIINFEKL tetramers. After incubation, cells were washed gently with PBS and were fixed and permeabilized using buffers from eBioscience (Intracellular fixation buffer and intracellular permeabilization buffer). This was followed by blockade with 5% FBS in permeabilization buffer. Cells were stained with mouse anti-galectin 3 (Thermofisher)

and rabbit anti-Zap70 (Cell Signaling Technology) for 2 hrs at room temperature.

After washing, cells were stained for 30 minutes with anti-mouse alexa fluor 568

(Thermofisher) and anti-rabbit alexa fluor 488 (Thermofisher). Thereafter cells were

washed and mounted with fluoromount (Sigma Aldrich).

Activation of CD8^{+} T cells with peptide pulsed APCs

APCs were generated from the bone marrow of C57BL/6 mice, using IL-4 and GM-

CSF as described (Sehrawat et al., 2013). $1x10^5$ APCs were placed on poly-lysine-

treated coverslips and pulsed with SIINFEKL peptide (1µg/ml) for 2 hrs at 37°C.

$4x10^5$ purified OT1 CD8^{+} T were co-cultured with peptide-pulsed BMDCs for upto an

hr. Cells were then stained as described in the previous section and analyzed by

confocal microscopy.

In vivo **activated cells analysis by immunofluorescence microscopy**

$5x10^4$ or $1x10^5$ purified CD8^{+} T cells from OT1 mice were adoptively transferred into

gender-matched C57B/6 mice. Subsequently, mice were infected intranasally with

$2x10^5$ pfu of MHV68-M2-SIINFEKL virus. At 6 or 55 dpi, mediastinal lymph nodes

were collected and a single cell suspension was prepared. Cells were stained with

class I MHC tetramer and were sorted by FACS. For some experiments, animals

were infected with WSN-SIINFEKL and H-2K[b]-SIINFEKL-specific CD8^{+} T cells were

isolated at 6 or 40dpi using magnetic beads coated with SIINFEKL-class I MHC

monomers. Briefly, one mg of M-270 streptavidin magnetic Dynabeads (In vitrogen)

were incubated with 10 µg of biotinylated H-2K[b] monomers, that were generated

using UV cleavable peptide for two hours at 4°C with gentle shaking (5 rpm). After

incubation, one ml of cold PBS was added gently and the beads were magnetically

separated. The washing of monomers coated beads was repeated three times.

Subsequently, the photocleavable ligand was exchanged with SIINFEKL peptide by

UV exposure at 365nm for 60 min and three washings were performed subsequently

to remove of any aggregated proteins. The H-2K[b]-SIINFELK coated beads thus

prepared were mixed with $10x10^6$ lymphocytes obtained from the single cell

suspension of spleens and mediastinal LN of virus infected mice. Beads and cells were incubated at 4°C for 90 min with gentle shaking (5rpm). Three times washing was performed with cold PBS using magnetic separation apparatus. The complex of beads and specific cells were added on polylysine-coated coverslips for 10 minutes at 37°C. Specific cells bound with beads were stained for galectin-3, Zap70 and DAPI for their subsequent analysis by confocal microscopy. The efficiency of sorting was ascertained cytofluorimetrically.

Generation of BMDCs

Bone marrow cells were isolated from the long bones of C57BL/6 mice. Cells were cultured with IL-4 (10ng/ml) and GM-CSF (10ng/ml) for four days in a humidified CO_2 incubator at 37°C. After differentiation cells were analyzed by flow cytometery, using anti-CD11b, CD11c and Class II MHC antibodies. More than 70 percent of cells were differentiated into DCs, as judged by expression of CD11c and activation associated molecules such as CD80, CD86 and Class II MHC.

Proliferation of cells

MACS-purified $CD8^+$ T cells from galectin-3 KO and WT animals were labeled with CFSE using protocols described elsewhere (Sehrawat et al., 2012). Labeled cells were stimulated with plate-bound anti-CD3 (1µg/ml) and soluble anti-CD28 (1µg/ml) for varying times. Cells were then collected, washed and stained on ice with the indicated fluorochrome-labeled antibodies. After multiple rounds of washing with FACS buffer, cells were analyzed by flow cytometry. Culture supernatants were collected to measure secreted cytokines. To assess the influence of extracellular galectin-3 on the proliferation of $CD8^+$ T cells, 10×10^6 OT1 cells were labeled with 2.5µM CFSE and 2×10^5 of labeled cells were stimulated with plate bound anti-CD3 (1ug/ml) and soluble anti-CD28 (1µg/ml) antibodies in the presence or absence of anti-galectin-3 neutralizing antibody (10µg/ml). Cells were incubated at 37°C and CFSE dilution was measured at different time points.

ELISA for cytokine measurement

Culture supernatants were collected from stimulated cells, supplemented with a protease inhibitor cocktail (Roche Diagnostics) and stored at -20°C until use. The levels of IL-2 in the culture supernatants were measured by sandwich ELISA using the OptEIA kit for mouse IL-2 (BD Bioscience).

Extraction of lung tissue for virus titration

Lung tissues were collected from WT and Gal-3 KO mice infected intranasally with 5×10^{5} pfu of MHV-68 and euthanized by CO_2 asphyxiation six days post-infection. Blood vessels just above the liver were cut and mice were perfused with 10-15 ml of sterile PBS by inserting a 25G needle into the right ventricle of the exposed heart. Lung tissues were weighed and frozen until use. Prior to titration of virus on 3T12-3 cells, lung tissues were thawed and homogenized with 500μl of DMEM without serum.

Statistical analysis

Student's "t" test and ANOVA tests were applied for statistical analysis to compare responses between groups, as indicated in the figure legends. The results are presented as mean ± SD. The p values are shown in the figures or figure legends and are represented as *$p \leq 0.05$, **$p \leq 0.01$, or ***$p \leq 0.001$.

Supplementary references

Altman, J.D., Moss, P.A., Goulder, P.J., Barouch, D.H., McHeyzer-Williams, M.G., Bell, J.I., McMichael, A.J., and Davis, M.M. (1996). Phenotypic analysis of antigen-specific T lymphocytes. Science *274*, 94–96.

Bakker, A.H., Hoppes, R., Linnemann, C., Toebes, M., Rodenko, B., Berkers, C.R., Hadrup, S.R., van Esch, W.J.E., Heemskerk, M.H.M., Ovaa, H., et al. (2008). Conditional MHC class I ligands and peptide exchange technology for the human MHC gene products HLA-A1, -A3, -A11, and -B7. Proc. Natl. Acad. Sci. U. S. A. *105*, 3825–3830.

Demetriou, M., Granovsky, M., Quaggin, S., and Dennis, J.W. (2001). Negative regulation of T-cell activation and autoimmunity by Mgat5 N-glycosylation. Nature *409*, 733–739.

Dunn, K.W., Kamocka, M.M., and McDonald, J.H. (2011). A practical guide to evaluating colocalization in biological microscopy. AJP Cell Physiol. *300*, C723–C742.

Pavlopoulos, G.A., Secrier, M., Moschopoulos, C.N., Soldatos, T.G., Kossida, S., Aerts, J., Schneider, R., and Bagos, P.G. (2011). Using graph theory to analyze biological networks. BioData Min. *4*, 10.

Sehrawat, S., Kirak, O., Koenig, P.-A., Isaacson, M.K., Marques, S., Bozkurt, G., Simas, J.P., Jaenisch, R., and Ploegh, H.L. (2012). CD8(+) T cells from mice transnuclear for a TCR that recognizes a single H-2K(b)-restricted MHV68 epitope derived from gB-ORF8 help control infection. Cell Rep. *1*, 461–471.

Sehrawat, S., Koenig, P.-A., Kirak, O., Schlieker, C., Fankhauser, M., and Ploegh, H.L. (2013). A catalytically inactive mutant of the deubiquitylase YOD-1 enhances antigen cross-presentation. Blood *121*, 1145–1156.